Anisotropic quantum dots: Correspondence between quantum and classical Wigner molecules, parity symmetry, and broken-symmetry states

B. Szafran,[1,2] F. M. Peeters,[1] S. Bednarek,[2] and J. Adamowski[2]
[1]*Departement Natuurkunde, Universiteit Antwerpen (Campus Drie Eiken), B-2610 Antwerpen, Belgium*
[2]*Faculty of Physics and Nuclear Techniques, AGH University of Science and Technology, al. Mickiewicza 30, 30-059 Kraków, Poland*
(Received 7 November 2003; published 30 March 2004)

We study electron systems confined in anisotropic quantum dots at high magnetic fields using the configuration-interaction scheme with a multicenter basis of single-electron functions centered around different sites. Elliptical, triangular, and square quantum dots are investigated. We study the relation between the quantum and classical charge density and conclude that at high magnetic field the quantum charge density reproduces all the equivalent lowest-energy configurations of classical point charges. Quantum systems with a classical counterpart of a unique lowest-energy configuration exhibit a smooth convergence of the charge density to the classical limit at high magnetic field. In quantum systems with several equivalent classical configurations the magnetic field induces discontinuous transformations of the ground-state symmetry associated with crossings of the corresponding few-electron energy levels. A linear combination of states with the crossing levels yields a semiclassical charge density with a broken symmetry. At the magnetic field corresponding to the level crossing this combination is an exact eigenstate of the Hamiltonian. For circular dots the present findings give an additional insight into the properties of the magic-angular-momenta states and into the physics behind the broken-symmetry mean-field solutions.

DOI: 10.1103/PhysRevB.69.125344 PACS number(s): 73.21.−b, 73.22.Gk

I. INTRODUCTION

Quantum dots[1] provide a convenient testing ground for studying electron localization in potentials which can be, to a certain extent, formed at will by proper etching techniques or chosen geometry of the applied gate electrodes. One of the most interesting problems in this field is the Wigner crystallization of the electron system induced by a high magnetic field. The problem of Wigner crystallization in cylindrical quantum dots[2–4] has been widely discussed and at present seems to be well understood both quantum mechanically and classically.[5] Wigner crystallization, i.e., the separation of electrons, in cylindrically symmetric potential appears in the inner coordinates of the system and the charges of separate electrons are not distinguishable in the rotationally invariant electron density. Therefore, in cylindrical quantum dots methods[6] based on charge-density measurements are not appropriate for the observation of Wigner crystallization. However, such an approach is possible in structures of lower symmetry. Previous exact diagonalization studies of a three-electron system in a triangular quantum dot[7] and of a system of six electrons in an elliptical quantum dot[8] showed that Wigner crystallization can be observed in the charge-density distribution of the electrons in the laboratory frame. Moreover, an exact study of the two-electron system has been presented[9] for triangular, square, and hexagonal quantum dots in the absence of a magnetic field and in an elliptical dot at zero magnetic field.[10] Wigner crystallization of few-electron systems in large polygonal quantum dots in the absence of an external magnetic field was studied using density-functional theory.[11–13] This theory was also applied to evaluate the addition spectra in elliptical quantum dots.[14] The addition spectra of elliptical dots have been studied with Hartree-Fock method[15] as well. The effect of pinning of the Wigner molecule by a Gaussian impurity perturbation in an isotropic confinement potential was recently studied by the quantum Monte Carlo approach.[16,17]

In this paper we perform a detailed study of the charge density of two-, three-, and four-electron systems confined in anisotropic potentials using an exact diagonalization approach. We consider elliptical, square, and triangular shaped quantum dots and investigate the magnetic-field-induced Wigner crystallization. A relation between the quantum and classical charge distributions in anisotropic structures[18] is found. In particular we discuss the high-magnetic-field behavior of quantum systems whose classical counterparts possess several equivalent lowest-energy configurations.

A lot of attention was paid[2,3] to the problem of the sequence of the ground-state angular momenta after the maximum density droplet[19] (MDD) breakdown in cylindrical quantum dots. The magnetic field increases the absolute value of the angular momentum of the confined electron system, but only certain angular momenta with magic quantum numbers[2,3,20–22] are realized. For the magic angular momenta the classical symmetry is reproduced in the inner coordinates of the quantum system[2] and the electron-electron interaction energy as a function of the angular momentum presents local minima.[23] At the end of this paper we point out a relation between the magic angular momenta and the charge density in the laboratory frame. We also consider the magnetic-field-induced parity transformations in elliptical dots which are less thoroughly studied counterparts of the angular-momentum transitions appearing in circular dots.

To discuss the charge-density distribution the application of an exact diagonalization method is crucial since mean-field approaches may lead to an artifactal breaking of the symmetry of the confinement potential.[3] The broken-symmetry solutions present a semiclassical type of localization. On the other hand we found[24] recently that in the

strictly infinite magnetic-field limit the energy of the broken-symmetry solution with semiclassical localization becomes equal to the energy of the exact solution. In this paper we study the realistic case of high but finite magnetic fields and extend our previous work to anisotropic confinement potentials. In particular, we reconsider the problem of the symmetry breaking at the exact diagonalization level and demonstrate that a construction of the exact broken-symmetry solution of the few-electron Schrödinger equation is possible for certain values of the magnetic field.

Some of the previous studies of Wigner crystals[25–27] and Wigner molecules[23,24,28,29] used a multicenter basis of the single-electron lowest-Landau-level functions. However, these calculations[23–29] used Hartree-Fock or similar approaches. In the present paper, we use the single-electron multicenter basis for the construction of the configuration-interaction approach which allows for an exact solution of the Schrödinger equation for few-electron systems confined in potentials of arbitrary symmetry. This approach is a generalization of the single-configurational multicenter Hartee-Fock (MCHF) method[24,29] which we elaborated previously.

The paper is organized as follows. The second section describes the multicenter-configuration-interaction method as applied in this paper as well as presents test calculations for circular dots. Sections III, IV, and V contain discussion of results obtained for elliptical, square, and triangular dots, respectively. The conclusions reached for lower-symmetry structures are discussed in the context of circular dots in Sec. VI. Summary and conclusions are given in Sec. VII.

II. MULTICENTER-CONFIGURATION-INTERACTION METHOD

We consider N electrons confined in a two-dimensional (x,y-plane) quantum dot subject to a strong external magnetic field oriented parallel to the z axis. We solve the N-electron Schrödinger equation with the Hamiltonian

$$H=\sum_{i=1}^{N} h_i+\sum_{i=1}^{N}\sum_{j>i}^{N}\frac{\kappa}{r_{ij}}+BS_z g^*\mu_B, \tag{1}$$

where h stands for the single-electron Hamiltonian,

$$h=\frac{1}{2m^*}(-i\hbar\boldsymbol{\nabla}+e\mathbf{A})^2+V(x,y), \tag{2}$$

g^* is the effective Landé factor, S_z the z component of the total spin, B the magnetic field, μ_B stands for the Bohr magneton, $\kappa=e^2/4\pi\epsilon_0\epsilon$, ϵ is the dielectric constant and m^* the electron effective mass. We use the Landau gauge $\mathbf{A}=(-By,0,0)$ and adopt material parameters for GaAs, i.e., $m^*/m_0=0.067$, $\epsilon=12.9$, and $g^*=-0.44$.

We assume complete spin polarization of the electron system by the external magnetic field. The multicenter-configuration-interaction (MCI) scheme is constructed in the following way. First we diagonalize the single-electron Hamiltonian (2) in a multicenter basis

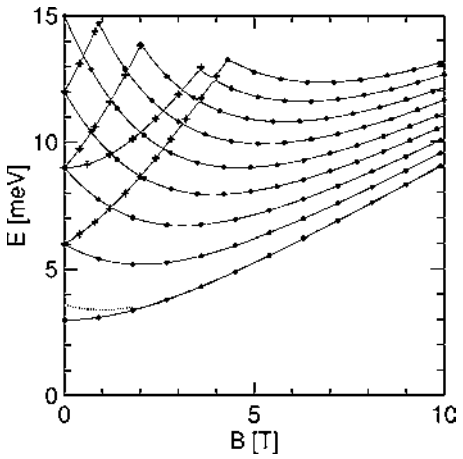

FIG. 1. The single-electron spectrum calculated with the trial wave function (3) for an isotropic quantum dot with $\hbar\omega=3$ meV (solid lines). Eleven centers have been used, one located at the origin and the others at the circumference of a circle with variationally optimized radius. Symbols show the exact Fock-Darwin energy levels corresponding to the lowest (dots) and higher bands (crosses). The dotted line shows the estimate for the ground-state energy obtained when the center located at the origin is excluded from the basis.

$$\Psi_\mu(\mathbf{r})=\sum_{i=1}^{M} c_i^\mu \psi_{\mathbf{R}_i}(\mathbf{r}), \tag{3}$$

with

$$\psi_{\mathbf{R}}(\mathbf{r})=\sqrt{\frac{\alpha}{2\pi}}\exp\left\{-\frac{\alpha}{4}(\mathbf{r}-\mathbf{R})^2+\frac{i\beta}{2}(x-X)(y+Y)\right\}, \tag{4}$$

where $M\geqslant N$ is the number of centers $\mathbf{R}=(X,Y)$. Next, the N-electron Hamiltonian (1) is diagonalized in a basis of $M!/N!(M-N)!$ Slater determinants constructed from the single-electron orthonormal eigenvectors Ψ_μ (3) with $\mu=1,\ldots,M$. The position of the centers $\mathbf{R}_i$, α, and β are nonlinear variational parameters optimized for the total energy of the N-electron system. For three or more centers per electron the optimal value of the parameter β tends to $eB/\hbar$. At high magnetic field the parameter α also takes this value independently of M. For $\alpha=\beta=eB/\hbar$ the wave function (4) is the lowest-Landau-level eigenfunction.

The flexibility of the single-electron basis was verified for an isotropic parabolic potential $V(x,y)=m^*\omega^2(x^2+y^2)/2$, with $\hbar\omega=3$ meV. Solid lines in Fig. 1 show the magnetic-field dependence of the single-electron spectrum calculated with the trial wave function (3) with ten centers located at the circumference of a circle with equal angular spacings and the 11th center located at the origin. The radius of the circle was optimized variationally. The dots in Fig. 1 show the exact Fock-Darwin energy levels corresponding to the lowest band which at high magnetic field converges to the lowest Landau level. The crosses mark the energies of the higher Fock-Darwin bands. The present calculations with wave function (3) reproduce the exact single-electron spectrum

with a high precision. It is interesting to note that the basis (3) constructed of the displaced lowest-Landau-level wave functions (4) reproduces also higher Fock-Darwin bands. Since we are using the Landau gauge the single-electron wave functions (3) are not eigenfunctions of the angular-momentum operator. However, for all the plots presented in Fig. 1, the expectation values of the angular momentum calculated for the wave functions (3) reproduce exactly the correct eigenvalues.

The exact ground Fock-Darwin state wave function possesses the form (4) with $X=Y=0$. The dotted line in Fig. 1 shows the variational estimate of the ground-state energy obtained when the center at the origin is excluded from the basis. The related overestimation of the ground-state energy is nonzero only at low magnetic field ($B \lesssim 2.2$ T). We have found that the center located at the origin has no influence on the energy estimates for the single-electron states with nonzero angular momentum. Its contribution to the energy of the excited *s* states tends to zero at higher magnetic field similarly as for the ground state.

We have performed further tests for the isotropic harmonic confinement potential in order to verify the reliability of the present configuration-interaction approach to the few-particle states at high magnetic field. The results were compared with the standard exact diagonalization method with a basis constructed from the Fock-Darwin states of definite angular momentum.[24,30] The reference method[24,30] assumes neither spin polarization nor the occupation of the lowest Landau level and for $N \leqslant 4$ allows for nearly exact evaluation of the total energy.

Figure 2(a) shows the comparison of the exact total angular momentum of the three-electron system and the expectation values obtained with the MCI wave function for various number of centers placed on a circumference of a circle with equal angular spacings. The plot starts for $B=3$ T for which the ground state is the spin-polarized MDD.[19] The MDD decays at $B=4.6$ T [cf. black dots in Fig. 2(a)] to a nonpolarized state with angular momentum $-5\hbar$. For $B>5.4$ T the ground state of the three-electron system is spin polarized. Then, the angular momentum takes the magic values[2,3,20–22] and changes by $3\hbar$ as the magnetic field increases.

The present method with $M=N$ uses only a single configuration and at high magnetic field is equivalent to the multicenter HF method.[29] For $M=N=3$ the MCI method reproduces the angular momentum of the MDD state [cf. squares in Fig. 2(a)]. After the MDD decay, the expectation value decreases linearly with B in contrast to the exact stepwise decrease. The MCI method with six centers reproduces also the exact angular momentum of the first spin-polarized state after the MDD decay, and at higher magnetic fields it starts to decrease linearly with B. For $M=12$ the MCI method yields correct expectation values of the angular momenta of all spin-polarized states in the entire considered range of magnetic fields.

Let us now discuss the convergence of the energy estimates obtained with the MCI method to the exact ground-state energy [cf. Fig. 2(b)]. The overestimation of the exact energy with a single configuration [$M=N=3$, cf. the uppermost curve of Fig. 2(b)] is a nonmonotonous function of B. The oscillations are due to the fact that the energy estimate of MCI with $M=N$ is a smooth function of B, while the exact energy exhibits cusps at these values of B for which the ground-state angular momentum changes. The envelope of these oscillations decreases to 0 in the infinite magnetic-field limit.[24] Introduction of six centers reduces the overestimation of the total energy as long as the total angular momentum is reproduced by the MCI method with $M=6$ [cf. dashed line in the upper panel of Fig. 2(a)]. At higher magnetic field, for which the overlaps of functions (4) centered around different sites vanish, the precision of the MCI method with $M=6$ deteriorates to the one obtained with $M=3$, i.e., to the MCHF method.[29] The method with $M=9$ (12) centers gives the exact energy to a precision better than 0.15 meV (0.05 meV) for $5.4<B<20$ T, i.e., in the studied range of magnetic field after the MDD breakdown for which the adopted assumption of spin polarization is fulfilled. Results of similar test calculations for $N=2$ and 4 show that the corresponding upper bounds for the precision of the MCI method with three centers per electron ($M/N=3$) equal 0.1 and 0.12 meV, respectively.

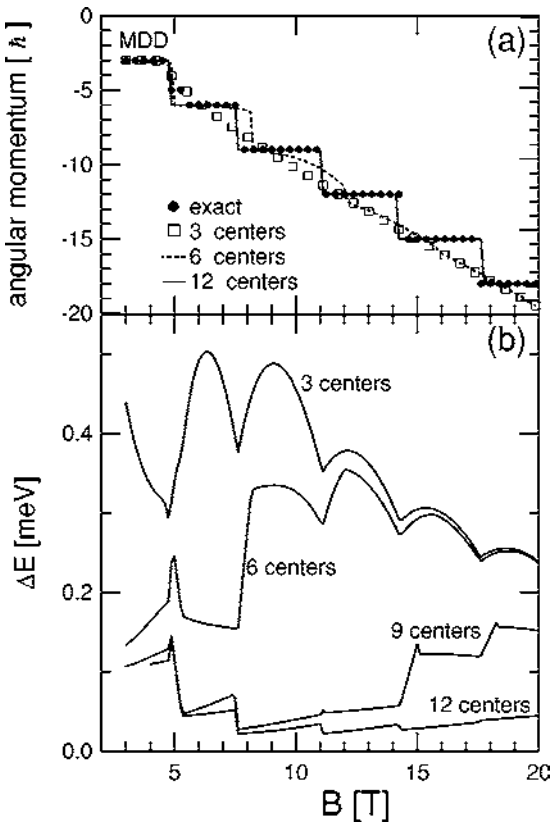

FIG. 2. (a) Exact total angular momentum of the ground state of the three-electron system confined in an isotropic quantum dot with $\hbar\omega=3$ meV and the expectation values for the multicenter-configuration-interaction wave functions using various number of centers. (b) The overestimation of the total three-electron energy with the multicenter approach for different number of centers.

Figure 3 shows the charge density of the three-electron system at $B=6$ T for three, six, and nine centers. In the single-configuration charge density ($M=3$) the circular

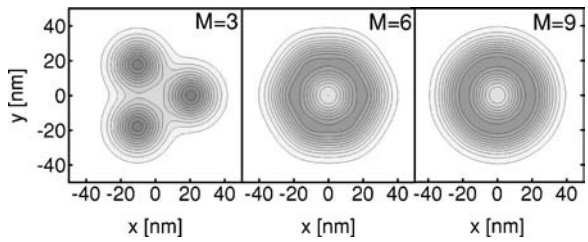

FIG. 3. MCI charge density obtained for the three-electron system with different M for $\hbar\omega=3$ meV and $B=6$ T. The darker the shade of gray the larger the electron density.

symmetry of the external potential is broken. For six centers the cylindrical symmetry is approximately restored, although at a closer inspection the sixfold symmetry—a trace of the choice of centers—can be noticed. For $M=9$ the charge density shows a perfect cylindrical symmetry. The present numerical method restores the cylindrical symmetry in a manner alternative to the rotated-electron-molecule approach of Yannouleas and Landman.[23]

We conclude that the single-electron wave functions (3) used in the present MCI approach work similarly as the Fock-Darwin functions with definite angular momentum (cf. Figs. 1 and 2). At high magnetic fields the precision of the MCI method is not worse than the MCHF method[29] which in turn gives exact results in the infinite magnetic-field limit.[24] The applicability of the present configuration-interaction approach is not limited to cylindrically symmetric potentials. The MCI method allows for a flexible choice of the position of centers which can be tailored to any smooth external potential of arbitrary profile and symmetry.

III. ELLIPTICAL QUANTUM DOT

A. Wigner crystallization

In this section we applied the MCI method to analyze Wigner crystallization in elliptical quantum dots with anisotropic parabolic potential $V(x,y)=m^*(\omega_x^2x^2+\omega_y^2y^2)/2$ with $\omega_y>\omega_x$. Calculations were performed with $M=12$ centers put on an ellipse symmetric with respect to the x and y axes with equal angular spacings.

Figure 4 shows the calculated charge densities for two-, three-, and four-electron systems at different magnetic fields (the energies obtained are listed in Table I). The lowest panel shows the position of the classical point charges in the lowest-energy configurations. The classical two- and four-electron systems in the studied potential possess a unique lowest-energy configuration. On the other hand the classical system of three electrons possesses two equivalent configurations (marked by ''black'' and ''white'' symbols in the lowest panel of Fig. 4). Existence of several equivalent classical configurations will be referred to as *classical degeneracy*.

At relatively low magnetic field (4 T) the electron puddles look very similar and exhibit two maxima at their left and right (x) ends. For $B=8$ T the electrons in the two- and four-electron systems start to become spatially separated. At higher magnetic field the electron charge densities for $N=2$ and 4 tend to the charge distributions of their classical

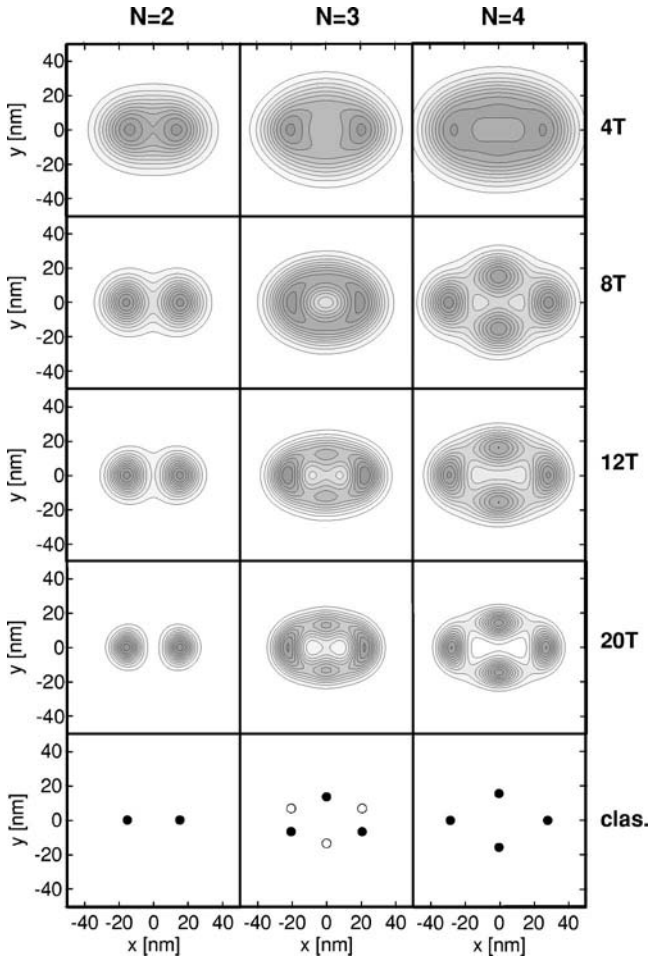

FIG. 4. Charge density of two-, three-, and four-electron systems for an anisotropic parabolic potential with $\hbar\omega_x=3$ meV and $\hbar\omega_y=4$ meV for different magnetic fields. The lowest panel presents the lowest-energy configurations of the classical point-charge systems. For $N=3$ the two energy-equivalent configurations are marked with full and open circles.

counterparts (cf. lowest panel of Fig. 4), which results from the shrinkage of the Landau radius with growing magnetic field. For $B=8$ T a central hole in the three-electron charge density appears. The plots of the three-electron charge densities for 12 and 20 T (cf. Fig. 4) show an appearance of two smaller maxima of the charge density along the y axis. This is shown more clearly in Fig. 5 for the three-electron charge density at $B=30$ T. The two charge maxima at the x ex-

TABLE I. Total energy of the N-electron system E_N (in meV) confined in an anisotropic parabolic potential with $\hbar\omega_x=3$ meV and $\hbar\omega_y=4$ meV.

B(T)	E_2	E_3	E_4
4	15.35	30.33	49.29
8	20.99	39.02	60.71
12	27.20	48.20	72.94
16	33.71	58.04	85.95
20	40.33	67.95	99.29

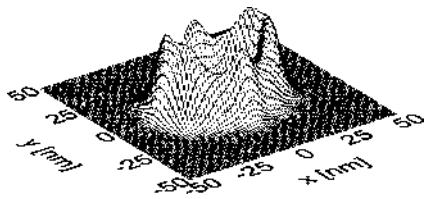

FIG. 5. Charge density of the three-electron system for an anisotropic parabolic potential with $\hbar\omega_x = 3$ meV, $\hbar\omega_y = 4$ meV, and $B = 30$ T.

tremities of the charge puddle are spread out along the y direction into two distinct maxima. The results of Figs. 4 and 5 show that the density distribution for the system of three electrons at high magnetic field tends to a linear combination of the two distributions of the degenerate classical configurations (cf. the lowest panel of Fig. 4).

Evidence of Wigner crystallization in the four-electron charge density is not always as apparent as in the case shown in Fig. 4. The left panel of Fig. 6 displays the charge density of the four-electron system at $B = 20$ T for $\hbar\omega_x = 3$ meV and different $\hbar\omega_y$. The right panel of the figure shows the corresponding configurations of the classical system.[18] The classical system possesses a single lowest-energy configuration for 3 meV$< \hbar\omega_y \lesssim 5.1$ meV with electrons situated along the x and y axes. For $\hbar\omega_y$ larger than 5.1 meV the electrons leave the axes and as a consequence two equivalent configurations appear. As $\hbar\omega_y$ is increased further the classical electrons become localized on the x axis and the classical degeneracy is removed. Note that the classical system exhibits a zigzag transition as discussed in more detail in Ref. 18. The classical configurations and the quantum charge distribution (cf. left panel of Fig. 6) are clearly related. In the absence of classical degeneracy ($\hbar\omega_y = 5$ and 9 meV) the quantum charge density possesses four nearly equal maxima localized close to the positions of the classical electrons in equilibrium. The plot for $\hbar\omega_y = 9$ meV represents a nearly one-dimensional case of a Wigner molecule,[31] in which the charge maxima at the ends of the puddle are slightly more pronounced than the maxima in its interior. A trace of the classical degeneracy for $\hbar\omega_y = 6$ meV in the quantum charge density is the elongation of the central maxima in the y direction. These central maxima for $\hbar\omega_y = 5.5$ meV merge into a single ringlike plateau with a hole in the center. For this special case the separation of electrons is not complete, since the charges of the two central electrons occupy the same island. We have found that in this case the separation of the two electrons cannot be observed even in the pair-correlation function[2] plots. Therefore, the four-electron system in this potential for $B = 20$ T presents an interesting case of *partial* Wigner crystallization.

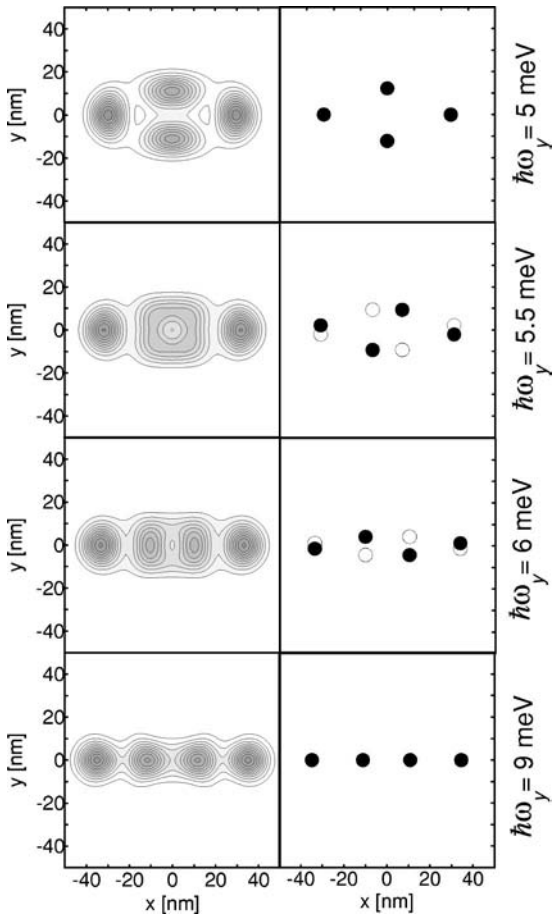

FIG. 6. Left panel: Charge density of the four-electron system at $B = 20$ T for $\hbar\omega_x = 3$ meV and different values of $\hbar\omega_y$. Right panel: Classical lowest-energy configurations. For $\hbar\omega_y = 5.5$ and 6 meV two equivalent configurations are marked with different symbols.

B. Parity symmetry

Let us now consider the spatial symmetry of the few-electron wave function in an elliptical dot. In an anisotropic confinement potential the angular momentum is no longer quantized. However, the wave functions of the few-electron systems in an elliptical dot have a definite parity with respect to the rotation by π angle. In cylindrical quantum dots the parity of the states is even (odd) if the angular momentum is an even (odd) multiple of $\hbar$. The MDD states for two, three, and four electrons have angular momentum equal to $-\hbar$, $-3\hbar$, and $-6\hbar$, respectively. Therefore, the two- and three-electron MDD states are of odd parity and the four-electron MDD state is of even parity. At magnetic fields above the MDD breakdown the angular momentum of the ground state takes the magic values[2,3,20–22] and changes by $N\hbar$. As a consequence the two- and four-electron systems in the MDD state and after its decay possess always the same parity (odd for $N = 2$ and even for $N = 4$), while for three electrons the parity changes with each ground-state transformation.

Solid lines in Fig. 7(a) show the two lowest-energy two-electron levels in the magnetic-field range corresponding to the MDD decay in a circular quantum dot. The displayed energy E' is calculated with respect to the lowest Landau level, i.e., $E' = E - N\hbar(\omega_c + S_z g^* \mu_B B) = E - 0.85(\text{meV/T}) \times NB$. The two-electron MDD decays at $B = 5.75$ T as the energy of the state with angular momentum $-3\hbar$ crosses the MDD energy level with $L = -\hbar$. The dashed lines present the magnetic-field dependence of the two lowest levels for an elliptical quantum dot with $\hbar\omega_x = 3$ meV and $\hbar\omega_y$

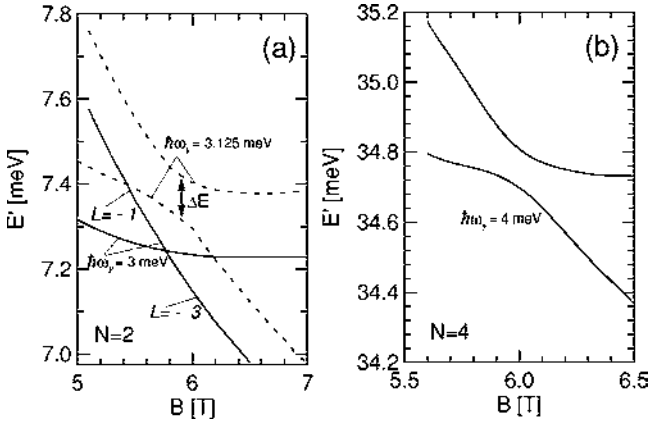

FIG. 7. Two lowest-energy levels of two (a) and four (b) electrons for $\hbar\omega_x = 3$ meV calculated with respect to the lowest Landau level as functions of the magnetic field.

$=3.125$ meV. Instead of a level crossing we observe an avoided crossing. The avoided crossing is due to the fact that the states involved are of the same odd parity. A similar avoided crossing related to the MDD decay in elliptical dot is observed for four electrons [cf. Fig. 7(b)]. Both the energy levels presented in Fig. 7(b) correspond to even parity states. For both $N=2$ and 4, further avoided crossings appear at higher magnetic fields. In the harmonic ellipsoidal quantum dot the center-of-mass motion separates from the relative motion eigenproblem.[32] If the energy levels involved in the avoided crossing corresponded to different center-of-mass states, the level crossing would still be observed in spite of the same parity of the considered few-electron states. The appearance of the avoided level crossings for $N=2$ and 4 indicates that these levels are associated with the same (ground) state of the center of mass. In the two-electron system the energy gaps between the anticrossing energy levels [ΔE, cf. Fig. 7(a)] for the same degree of anisotropy (ω_y/ω_x) are about four times larger than in four-electron systems. The extent to which the anisotropy mixes the magic-angular-momenta states of circular dots is a distinctly decreasing function of the differences of their angular momenta ($N\hbar$). The appearance of the avoided crossings in function of the anisotropy of the elliptical confinement in absence of a magnetic field has been discussed for an electron pair in Ref. 10.

The magnetic-field-induced ground-state transformations in the circular quantum dots are accompanied by cusps in the energy as a function of the magnetic field and stepwise changes of the angular momentum. Moreover, they appear along with discontinuous changes of the average size of the system,[30] the electron-electron interaction energy,[29] and abrupt transformations of the charge density. When the energy-level crossing is replaced by an avoided crossing (like in two and four elliptically deformed dots) the changes of physical quantities lose their sharp character and become continuous. As an illustration, a plot of the interaction energy in the two-electron system is presented in Fig. 8(a) for circular (solid line) and elliptical (dashed line) quantum dot. In the circular dot the interaction energy grows with magnetic field between the ground-state transformations which are accompanied by a stepwise decrease of this quantity. The interaction energy for the two-electron elliptical dot presents a smooth dependence on the magnetic field [cf. dashed line in Fig. 8(a)]. In circular quantum dots the sharp breakdown of the MDD is related with a level crossing leading to a sudden increase of the electron-electron correlation[30] and formation of a molecular configuration in the inner coordinates of the quantum system.[2,3,29,30] In the presence of the avoided crossings the formation of the Wigner phase becomes a continuous process.

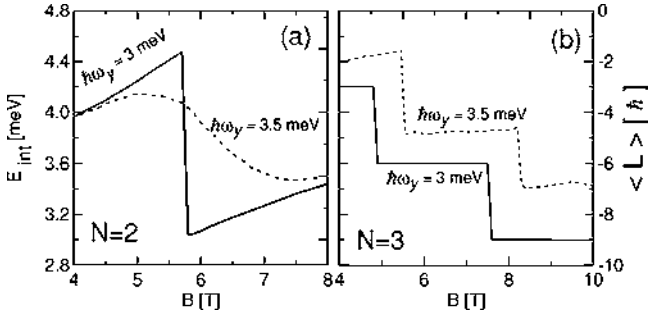

FIG. 8. Expectation value of the electron-electron interaction energy in the two-electron system (a) and of the angular momentum (b) in the three-electron circular ($\hbar\omega_x = \hbar\omega_y = 3$ meV—solid lines) and elliptical ($\hbar\omega_x = 3$, $\hbar\omega_y = 3.5$ meV—dashed lines) quantum dot.

In the three-electron system confined in an elliptical dot the magnetic-field-induced level crossings are still present because, like in circular dots, the subsequent ground states possess opposite parities. Figure 9 shows the two lowest-energy levels as function of the magnetic field. One of the two lowest-energy levels corresponds to the odd-parity state (solid line) and the other to the even-parity state (dashed

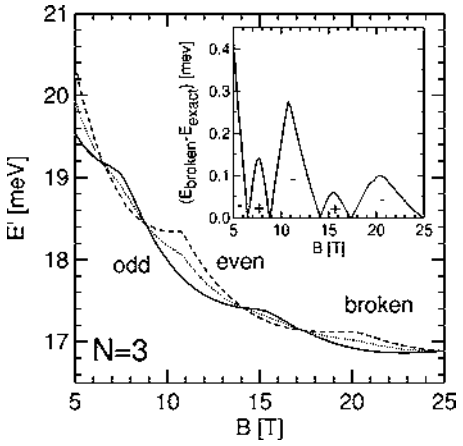

FIG. 9. Two lowest-energy levels of a three-electron elliptical dot ($\hbar\omega_x = 3$ meV, $\hbar\omega_y = 4$ meV) calculated with respect to the lowest Landau level. The energy level plotted with solid (dashed) line corresponds to the state of odd (even) parity. Dotted line shows the expectation value of the energy for the broken-symmetry state [cf. Sec. III C and Eq. (5)]. The inset presents half the energy spacing between the two energy levels, i.e., the energy overestimation by the expectation value of the Hamiltonian calculated for the broken-symmetry state (cf. Sec. III C). Signs "−" and "+" correspond to odd and even parity of the ground state, respectively.

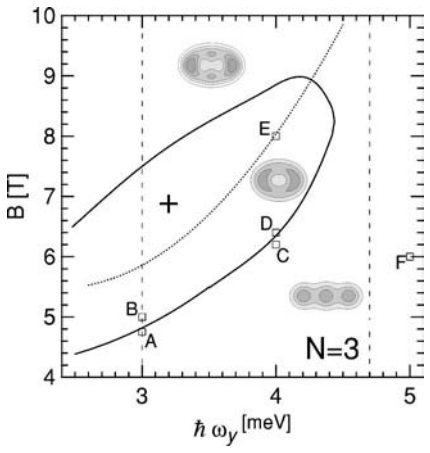

FIG. 10. Phase diagram for the parity of the three-electron spin-polarized ground state in an elliptical quantum dot for $\hbar\omega_x = 3$ meV. The parity is even in the region marked by a plus sign bounded by the solid line and odd outside of it. The dotted line shows the position of the avoided crossing of the lowest two odd-parity energy levels. The insets show schematically the qualitative picture of the charge density in the different phases. For the vertical dashed lines and the symbols, see text.

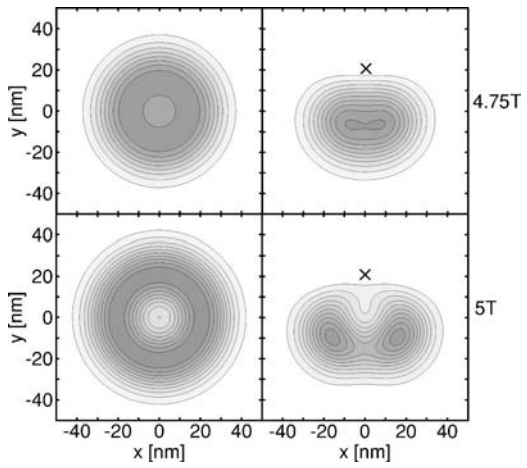

FIG. 11. Charge density (left panel) and PCF (right panel) plots for the three-electron system confined in a circular dot ($\hbar\omega_x = \hbar\omega_y = 3$ meV) in the MDD phase (upper panel cf. point marked by "*A*" in Fig. 10) and in the ground state with $L = -6\hbar$ appearing at higher magnetic field (lower panel cf. point marked by "*B*" in Fig 10. The position of one of the electrons in the PCF plot marked by $\times$ is fixed at point $x = 0$, $y = 21$ nm.

line). In the three-electron elliptical dot the changes of physical properties conserve their stepwise character as function of the magnetic field due to the parity transformations. Figure 8(b) shows the expectation value of the angular momentum for the three-electron system. Although, the angular momentum in an elliptical dot is not quantized, its expectation value presents discontinuous changes. For higher values of ω_y the angular momentum is quenched to zero as the confinement potential starts to resemble a quasi-one-dimensional wirelike dot.

Figure 10 shows the phase diagram for the parity of the spin-polarized three-electron system as a function of the strength of the y confinement and the magnetic field for $\hbar\omega_x = 3$ meV. The ground state is of even parity in the central region bounded by the solid line and marked by the "+" sign. The left vertical dashed line corresponds to circular symmetry of the confinement potential. The changes in the charge density occurring at the crossing of the border between the odd and even phases along this line are illustrated in Fig. 11. The upper panels of Fig. 11 show the charge density (left panel) and the pair-correlation function (PCF) (right panel) corresponding to the MDD phase in the point marked by "*A*" in Fig. 10. The lower panels correspond to the point marked by "*B*" in Fig. 10. Results of Fig. 11 show that the MDD decay is accompanied by the formation of a hole in the charge-density center[33] and a distinct growth of the electron separation in the inner coordinates presented at the PCF plots. Figure 12 displays the charge density and the PCF plots at the crossing of the border between the odd- and even-parity phases for elliptical dot with $\hbar\omega_y = 4$ meV (cf. the points marked by "*C*" and "*D*" in Fig. 10). The charge density in the even-parity ground state has a hole in the center, similarly as for the even-parity state in the cylindrical dot (cf. Fig. 11). An increase of the electron-electron correlation appearing at the crossing of the borders between the phases also resembles a similar effect appearing in circular dots (cf. right panel of Fig. 12). The charge-density plot for the same phase at a higher magnetic field ($B = 8$ T—point "*E*" in Fig. 10) was presented in Fig. 4. A qualitative change in the charge density is observed at higher magnetic fields when the next phase border is crossed. In the odd phase above this border, the two local maxima of the charge density appear at the y axis (cf. Fig. 4 for $B = 12$ T and $N = 3$). At higher magnetic field the charge density tends to reproduce both the degenerate classical configurations (cf. discussion of Fig. 4).

Figure 10 shows that with increasing anisotropy of the confinement the even-parity phase is pushed to higher magnetic fields and finally for $\hbar\omega_y > 4.4$ meV it is eliminated

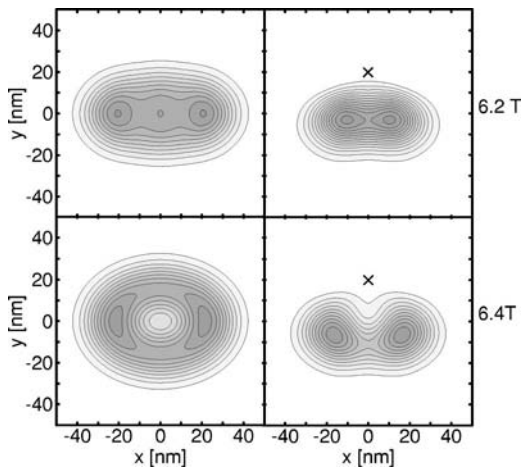

FIG. 12. Charge density (left panel) and PCF (right panel) plots for the three-electron system in an elliptical dot ($\hbar\omega_x = 3$ meV, $\hbar\omega_y = 4$ meV). The upper (lower) panel corresponds to the odd-(even-) parity state in the point marked by "*C*" ("*D*") in Fig. 10. The position of one of the electrons in the PCF plot marked by $\times$ is fixed at point $x = 0$, $y = 20$ nm.

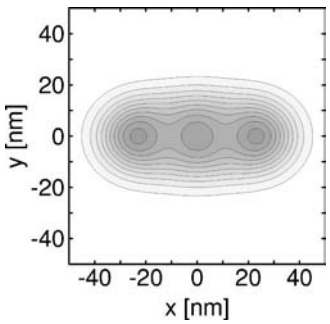

FIG. 13. Charge density for the three-electron system in an elliptical dot ($\hbar\omega_x=3$ meV, $\hbar\omega_y=5$ meV) for $B=6$ T. The plot corresponds to the point marked by "F" in Fig. 10.

from the phase diagram. The charge-density plot presented in the upper panel of Fig. 12 for point "C" in Fig. 10 shows that the odd-parity state forms a charge-density maximum in the center of the dot. The strong y confinement prevents the formation of the even-parity state (the lower panel of Fig. 12) in which this central charge-density maximum is removed. The right vertical dashed line in Fig. 10 marks the y confinement energy above which the zigzag structure[18] of the classical three-electron system (cf. lowest panel of Fig. 4) is suppressed to the x axis. Figure 13 shows the electron charge density plotted for $\hbar\omega_y=5$ meV and $B=6$ T (the point marked by "F" in Fig. 10). The observed three charge-density maxima at higher magnetic field shrink and tend toward the single nondegenerate classical configuration. In the quasi-one-dimensional regime of strong y confinement the convergence of the three-electron charge density to the classical limit is not accompanied by any level crossings.

C. Broken-symmetry states

The preceding results show that the quantum systems with classical degeneracy at high field contain all the classically degenerate configurations. As a consequence, the corresponding charge density does not resemble any single classical charge distribution. One has to break the symmetry of the external potential in order that the quantum charge density reproduces one of the degenerate classical configurations. Let us construct such broken-symmetry states ψ_{bs} in form of a linear combination of the two lowest-energy few-electron states (χ_1 and χ_2, respectively),

$$\psi_{bs}=(\chi_1+c\chi_2)/\sqrt{2}, \tag{5}$$

where $|c|^2=1$. Usually, the charge density of a state constructed in this way does not reproduce the symmetry of the confinement potential. We constructed such broken-symmetry states for the system of three electrons in an elliptical dot with $\hbar\omega_x=3$ meV and $\hbar\omega_y=4$ meV (cf. Fig. 9). We have found that the broken-symmetry charge density exhibits three maxima. For a properly chosen phase of the coefficient c in Eq. (5) the positions of these maxima coincide with the position of the electrons in one of the degenerate classical configurations (cf. the lowest panel of Fig. 4). Figure 14 shows the charge density of the broken-symmetry states for different values of the magnetic field. Plots in Figs.

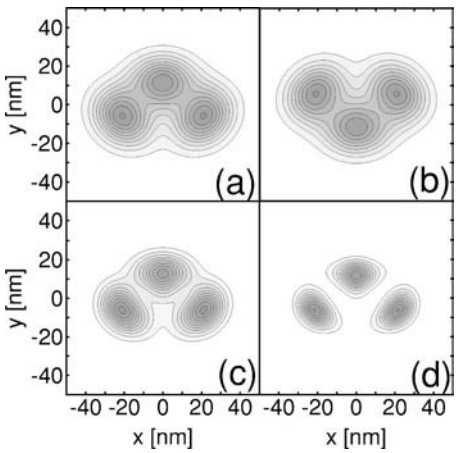

FIG. 14. Charge density of the broken-symmetry three-electron states [cf. Eq. (5)] in an elliptical dot ($\hbar\omega_x=3$ meV, $\hbar\omega_y=4$ meV) for $B=6.3$ T (a,b), 14.125 T (c), and 25 T (d). For the chosen fields the plots correspond to exact ground states.

14(a) and 14(b) correspond to "black" and "white" degenerate classical configurations depicted in the lowest panel of Fig. 4. Plots 14(a) and 14(b) have been obtained with opposite sings of c in formula (5), so they correspond to orthogonal wave functions. Figures 14(a), 14(c), and 14(d) show that as the magnetic field grows the charge density of the broken-symmetry state converges to one of the degenerate classical configurations of point charges.

The expectation value of the energy calculated for the broken-symmetry state [Eq. (5)], independently of the phase of c, is equal to the arithmetic average of the two lowest-energy levels. It means that this expectation value overestimates the exact ground-state energy by half of the energy spacing between the two lowest levels (cf. inset of Fig. 9). For the magnetic fields corresponding to degenerate χ_1 and χ_2 states [cf. Eq. (5)], i.e., to the energy-level crossings presented in Fig. 9, the broken-symmetry states (5) are exact ground eigenstates of the Hamiltonian. The magnetic fields chosen in Fig. 14 correspond to these level crossings. Therefore, the charge densities presented in this figure correspond to the exact ground-state solutions of the Schrödinger equation. Conversely, for an arbitrary value of the magnetic field the exact ground-state wave function can be constructed from a superposition of the wave functions of two broken-symmetry states with semiclassical electron localization [cf. Figs. 14(a) and 14(b)].

IV. SQUARE QUANTUM DOT

In order to verify the conclusions concerning the high-magnetic-field evolution of the charge density in elliptical dots we performed a study of Wigner crystallization in quantum dots with square and triangular confinement potentials. For the square quantum dot we used a smooth confinement potential with a square profile,

$$V(x,y)=\tfrac{1}{2}m^*\omega^2(x^2+y^2)[1+\cos(4\phi)/5], \tag{6}$$

where ϕ is the angle between the position vector (x,y) and the x axis. We take $\hbar\omega=3$ meV. The potential is illustrated

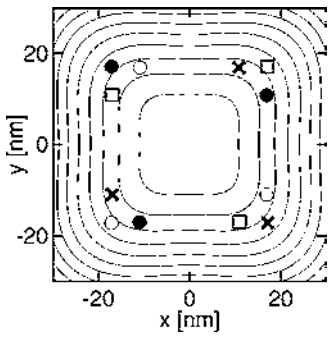

FIG. 15. Equipotential lines for the square confinement potential (6). The different types of symbols mark the position of the electrons in one of the four energy-equivalent configurations for the three-electron system.

in Fig. 15 along with the degenerate classical lowest-energy configurations of three electrons. On the other hand for two electrons there are only two equivalent configurations in which the electrons reside in the opposite corners of the square,[34] and for $N=4$ the classical system is nondegenerate with electrons occupying all the corners.

The MCI calculations for potential (6) have been performed with 12 centers placed on the circumference of a square with equal spacings along its sides. The size of the square was optimized variationally. The obtained charge density is presented in Fig. 16. In the system of four electrons the charge density becomes distinctly separated into four single-electron islands. For $N=2$ and 3 the formation of the charge maxima at the corners of the square appears with a pronounced delay in magnetic-field strength with respect to the four-electron system.

The PCF plot presented in Fig. 17 gives an additional insight into the electron distribution in the square quantum

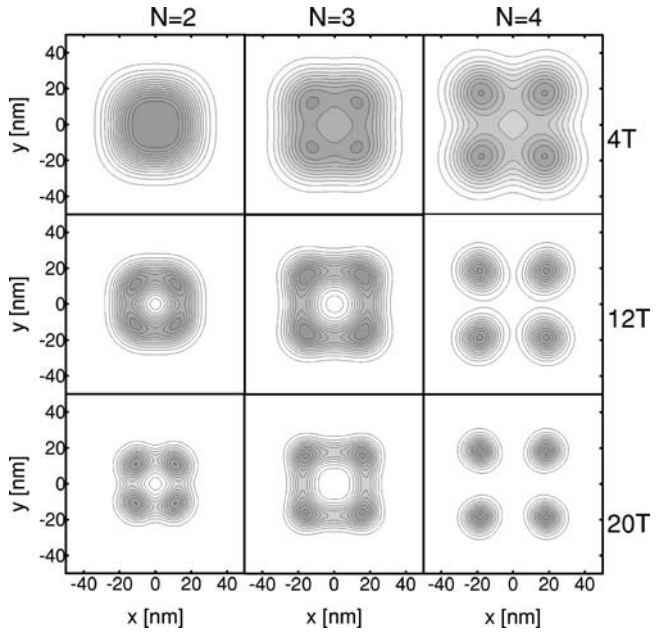

FIG. 16. Charge densities of two-, three-, and four-electron systems in the square quantum dot for various values of the magnetic field.

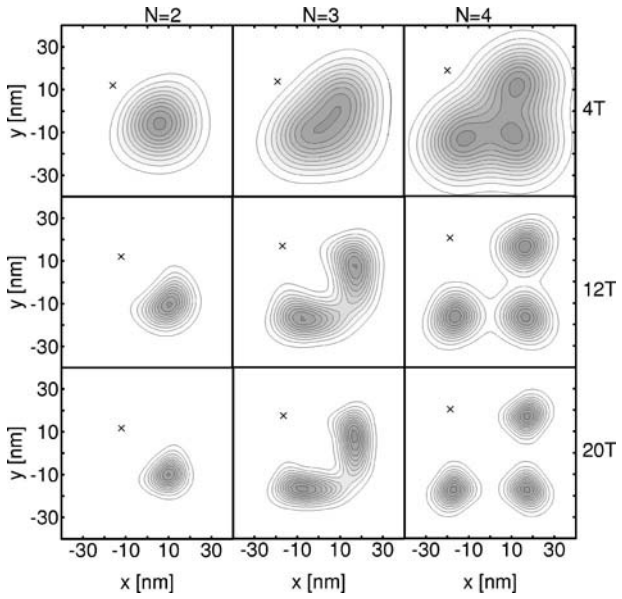

FIG. 17. Pair-correlation function for the two-, three-, and four-electron system in the square quantum dot. The cross marks the position of one of the electrons $[(-12,12),\ (-17,17),\ (-20,20)$ for $N=2,\ 3$, and 4, respectively (in nanometers)].

dot when one of the electrons is fixed (cross in Fig. 17) along one of the diagonals. At high magnetic field the plots for $N=2$ and 4 show that the other electrons become localized semiclassically at the corners of the square. On the other hand the two remaining electrons in the three-electron system are smeared out over the two opposite sides of the square and their localization is weaker than in the two- and four-electron systems. This weaker localization is related to the degeneracy of the classical three-electron system and to the fact that the electrons in the degenerate classical configurations occupy nearby positions.

Table II shows that the present MCI approach gives a decent convergence of the energy estimates even for the three-electron system whose localization in the square quantum dot is rather vicious.

The gathering of the electron density at the corners of the square dot that we observe at high magnetic field is in qualitative agreement with previous exact[9] and density-functional-theory[11,12] results for large quantum dots in the absence of magnetic field.

The symmetry of the electron states in square quantum dots is higher than in elliptical dots.[35] In the symmetric gauge the Hamiltonian eigenstates are also eigenstates of the

TABLE II. Convergence of the total energy (in meV) for the three-electron system in the square quantum dot (6) as function of the number of centers used in the wave function (3).

	M			
B(T)	4	8	12	16
4	28.51	28.08	27.99	27.98
12	48.87	46.38	46.27	46.26
20	70.22	66.35	66.12	66.08

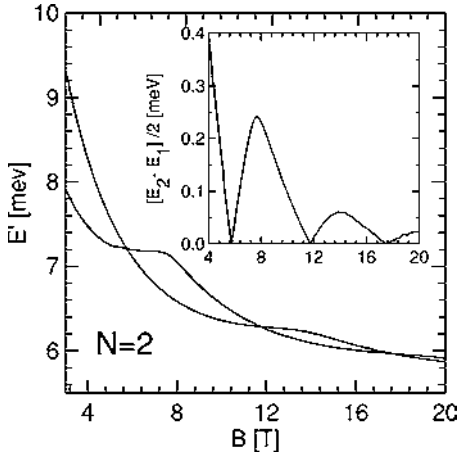

FIG. 18. Two lowest-energy levels of the two-electron square quantum dot calculated with respect to the lowest Landau level as functions of the magnetic field. Both energy levels are of odd parity. The inset shows half of the energy spacing between the two lowest-energy levels.

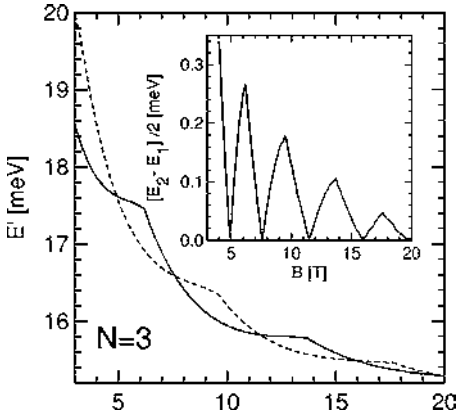

FIG. 19. Two lowest-energy levels of the three-electron square quantum dot calculated with respect to the lowest Landau level. The odd- (even-) parity energy level is plotted with solid (dashed) line. The inset presents the half of the energy spacing between the two lowest-energy levels.

$\pi/2$ rotation operator corresponding to eigenvalues ± 1 (even-parity states) and $\pm i$ (odd-parity states). Since we are using the Landau gauge, in which the Hamiltonian does not commute with the $\pi/2$ rotation operator, we cannot discuss these symmetries properly.[36] However, we have found that the ground state of two electrons for the MDD and the other spin-polarized ground states at high magnetic fields is always of odd-parity-like in circular and elliptical quantum dots. Figure 18 shows the two lowest-energy levels of two-electrons in a square quantum dot (the lowest excited state is also of odd parity). Contrary to the case of elliptical dots the crossings between the odd-parity energy levels are not avoided. Thus we can conclude that the interchanging two-electron energy levels presented in Fig. 18 correspond to orthogonal eigenstates with eigenvalues $\pm i$ of the $\pi/2$ rotation operator.

For three electrons the oscillations of the ground-state parity with magnetic field are observed like in circular and elliptically deformed dots (cf. Fig. 9). The two lowest-energy levels for $N=3$ are presented in Fig. 19.

The two- and three-electron systems in square quantum dots are similar to the three-electron system in an elliptically deformed dot (with comparable confinement energies in the x and y directions) in three points. First, all these systems exhibit classical degeneracy. Second, their energy levels exhibit crossings as function of the magnetic field (cf. Figs. 13, 18, and 19). Third, it is possible to extract a single semiclassical broken-symmetry charge distribution as a linear combination of the two crossing lowest-energy levels.

Figure 20 shows the charge density of a superposition of the two lowest-energy states of two- and three-electron square dot calculated using Eq. (5). The other semiclassical configuration of the two-electron system corresponding to electrons gathering at the other diagonal of the square can be obtained by changing the sign of c in Eq. (5). The three-electron charge density plotted in Figs. 20(c) and 20(d) corresponds to the classical charge density marked by squares in Fig. 15. The three other equivalent configurations can be obtained by rotating the coefficient c by $\pi/2$ in the Gauss plane. It is interesting to note that a linear combination of the two lowest-energy states can yield all four semiclassical charge distributions. On the other hand any pair of the four broken-symmetry states is sufficient to reconstruct the exact ground state. The broken-symmetry states corresponding to the classical configurations marked by squares and open dots (full dots and crosses) in Fig. 15 are mutually orthogonal. With increasing magnetic field the charge maxima presented in Fig. 20 shrink to the classical point-charge distributions.

The energy overestimate of the broken-symmetry state (half of the energy spacing between the lowest levels) is presented in the insets of Figs. 18 and 19, respectively. We notice that the envelope of the oscillation of the energy overestimate is a decreasing function of the magnetic field. Similar decreasing tendency can be noticed for the three-electron system in an elliptical dot (cf. inset of Fig. 9), but in that case the parity of the ground state has a visible influence on the height of the local maxima of the energy overestimate due to the shrinkage of the stability region of the even-parity phase with growing y-confinement energy (cf. Fig. 10).

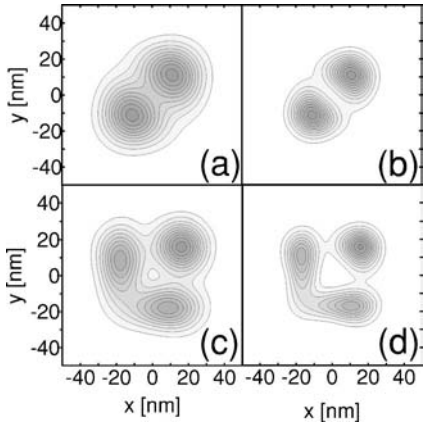

FIG. 20. Charge density of the broken-symmetry solutions [cf. Eq. (5)] of the two- (a, b) and three-electron square quantum dot, for $B=5$ T (a), 12 T (b), 8 T (c), and 16 T.

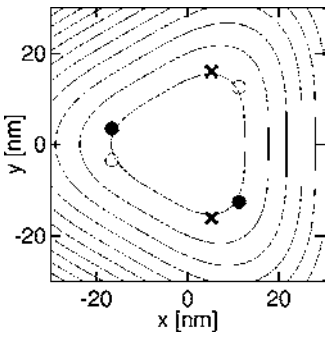

FIG. 21. Equipotential lines for the triangular confinement potential (7) with $\hbar\omega=3$ meV. Different symbols show the three degenerate classical lowest-energy configurations for the two-electron system.

The four-electron spin-polarized ground state in a square dot is of even parity (like in circular and elliptical dots) and no level crossings as function of the magnetic field are observed. In this respect the four-electron system confined in a square quantum dot is similar to the two- and four-electron systems in elliptical dots as well as to three-electrons in strongly deformed wirelike quantum dots (cf. discussion of Fig. 10). Another feature common to almost all these systems is that their classical counterpart is nondegenerate. The only exception is the four-electron system for elliptical dots with ω_y/ω_x ratio corresponding to the zigzag classical configuration (cf. Fig. 6). We did not obtain level crossing for this system, although for certain magnetic fields the excited odd-parity state can closely approach the even ground state.

V. TRIANGULAR QUANTUM DOT

The confinement potential for a triangular dot is taken as[7]

$$V(x,y)=\tfrac{1}{2}m^*\omega^2(x^2+y^2)[1+2\cos(3\phi)/7], \qquad (7)$$

with $\hbar\omega=3$ meV. Classical three- and four-electron systems in this potential are nondegenerate; the electrons occupy all the corners of the triangle, and one of the electrons in the four-electron system resides in the center of the triangle.[34] On the other hand the classical two-electron system is threefold degenerate. The profile of the potential and the positions of electrons in the degenerate two-electron classical configurations are presented in Fig. 21.

The calculations were performed with 12 centers situated at the circumference of an equilateral triangle with equal spacing along its sides. For four electrons an additional 13th center was introduced in the center of the triangle. As in the preceding calculations, the size of the triangle was optimized variationally. The obtained charge density is plotted in Fig. 22. In systems of three and four electrons the magnetic field induces the formation of single-electron islands around the positions of classical electrons in the nondegenerate lowest-energy configurations. The clear localization of electrons for $N=3$ and 4 resembles the one for four-electrons in the square quantum dot (cf. Fig. 16) as well as the plots for $N=2$ and 4 in the anisotropic confinement potential presented in Fig. 4. On the other hand for $N=2$ the formation of the

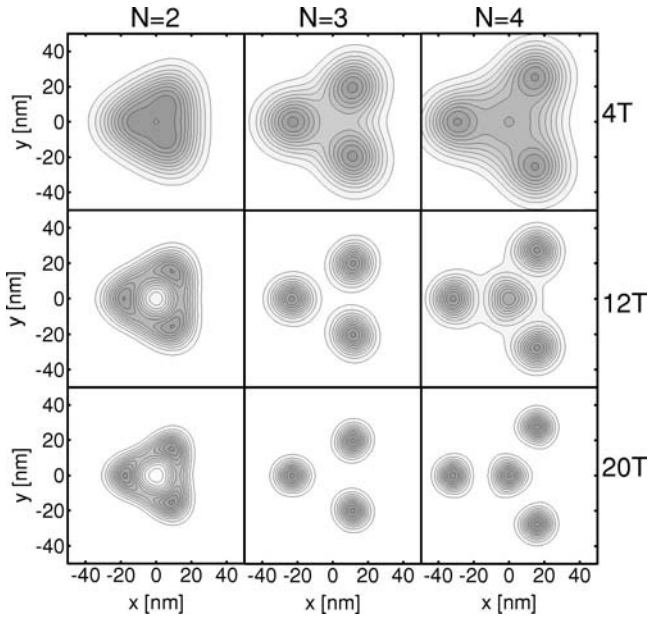

FIG. 22. Charge densities of two-, three-, and four-electron systems in a triangular quantum dot (7) with $\hbar\omega=3$ meV for various values of the magnetic field.

charge maxima at the corners of the triangle appears with a visible delay and the localization of electrons along the sides is observed like in the three-electron system in the square quantum dot (cf. Fig. 16).

The three- and four-electron systems in the triangular dot, for which their classical lowest-energy configuration is nondegenerate, do not exhibit any level crossings as function of the magnetic field, but the two-electron system (classically degenerate) does. The crossing lowest-energy levels are presented in Fig. 23. The electron systems in the triangular confinement potential do not possess a definite parity. However, (in the symmetric gauge) the Hamiltonian eigenfunctions should also be eigenstates of the $2\pi/3$ rotation operator cor-

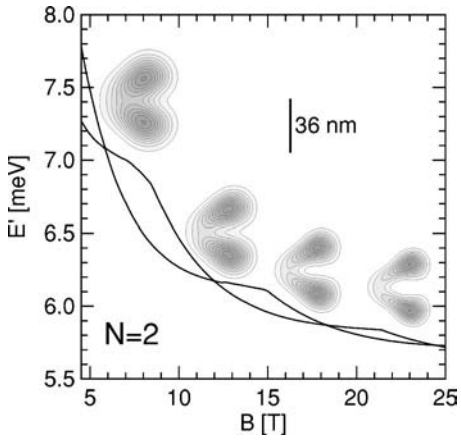

FIG. 23. Two lowest-energy levels of a two-electron triangular quantum dot calculated with respect to the lowest Landau level. The insets present the charge density of the broken-symmetry solutions obtained for the subsequent energy-level crossings appearing at magnetic fields 5.9, 12, 18.3, and 24.4 T, respectively. The bar in the inset shows the length scale for the charge-density plots.

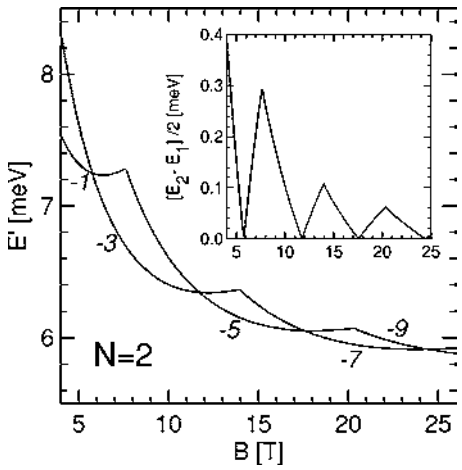

FIG. 24. Two lowest-energy levels of the two-electron system in circular dot with $\hbar\omega=3$ meV calculated with respect to the lowest Landau level. The numbers (-1, -3, -5, -7, and -9) give the angular momenta of the two lowest-energy states (in $\hbar$ units).

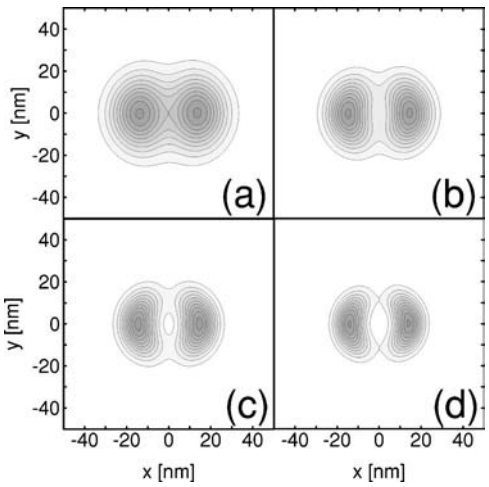

FIG. 25. Broken-symmetry charge densities of the superposition of two lowest-energy states for $N=2$ for a circular dot. Plots (a–d) correspond to magnetic fields 6, 11.5, 17.5, and 25 T, respectively.

responding to eigenvalues equal to three complex cubic roots of 1. It may be expected that each level of the crossing pairs presented in Fig. 23 corresponds to a different eigenvalue. Similarly as in the dots studied in the preceding part of the paper the energy spacings between the two lowest levels exhibit oscillations decreasing with the external field. Formula (5) still successfully produces the semiclassical charge-density distributions. The insets of Fig. 23 show the plots of the broken-symmetry solutions drawn for the magnetic fields corresponding to the level crossings. The presented charge densities correspond to the classical configuration marked by crosses in Fig. 21. We have verified that the other two semiclassical distributions can be obtained by rotation of c in Eq. (5) by $2\pi/3$ in the Gauss plane.

VI. EXACT BROKEN-SYMMETRY STATES FOR CIRCULAR DOTS

From the present findings for anisotropic dots we may wonder whether it is also possible to obtain the classical configurations for circular dots. The classical electron systems in circular dots are infinitely degenerate with respect to rotation over an arbitrary angle. From the point of view of the preceding discussion, the cylindrical symmetry of the exact charge density can be considered as a superposition of all classically degenerate configurations. Like most of the classically degenerate systems discussed in this paper, the electron systems in circular quantum dots exhibit level crossings as function of the magnetic field.

The two lowest-energy levels of the two-electron circular dot are displayed in Fig. 24. For an arbitrary magnetic field the ground and the first excited states correspond to adjacent magic angular momenta (given by numbers close to the curves in Fig. 24). The inset shows half of the energy spacing between the lowest levels. The superposition of the two lowest-energy states calculated according to Eq. (5) give the broken-symmetry semiclassical distributions which are displayed in Fig. 25. The magnetic fields chosen for Fig. 25 are close to the level crossings presented in Fig. 24. At the level crossings the broken-symmetry states are exact ground states. The corresponding charge densities shrink to pointlike density distributions with growing magnetic field. The modification of the phase of c in Eq. (5) results in a rotation of the broken-symmetry Wigner molecules, which can be pinned at an arbitrary angle for a properly chosen phase.[37] It is a striking feature of the quantum superposition [Eq. (5)] that for an arbitrary magnetic field the exact ground state with circularly symmetric charge density can be reconstructed from the wave functions of two broken-symmetry Wigner molecules pinned at any two different angles [cf. also the discussion in connection with Figs. 20(c) and 20(d)].

The energy levels of the three- and four-electron system (cf. Figs. 26 and 27) exhibit the same qualitative behavior as for $N=2$. The envelope of the lowest-energy-level separation presented for $N=2$, 3, and 4 electrons in the insets of Figs. 24, 26 and 27 exhibits very similar dependence on the magnetic field, however ''the frequency'' of these oscillations grows fast with the number of electrons. The broken-symmetry charge densities in the neighborhood of the

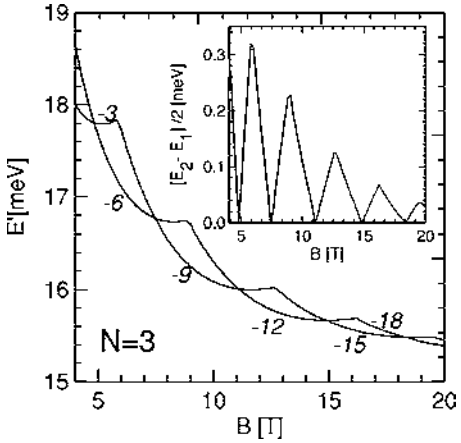

FIG. 26. Same as Fig. 24 but for $N=3$.

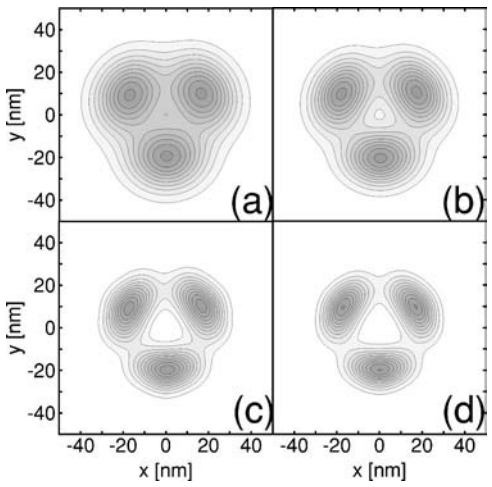

FIG. 27. Broken-symmetry charge densities for $N=3$ for a circular dot. Plots (a–d) correspond to magnetic fields 4.9, 7.5, 15, and 18.4 T, respectively.

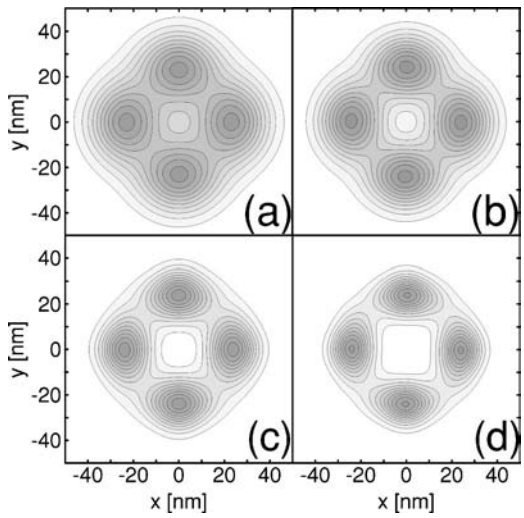

FIG. 29. Broken-symmetry charge densities for $N=4$ for a circular dot. Plots (a–d) correspond to magnetic fields 4.75, 6.5, 11.5, and 16 T, respectively.

ground-state level crossings for $N=3$ and 4 are displayed in Figs. 27 and 29. The charge density presented in Fig. 27(a) has been obtained as a superposition of states with angular momenta $-3\hbar$ and $-6\hbar$. The charge densities of these states in the neighborhood of their energy-level crossings were shown in Fig. 11.

The present broken-symmetry charge densities, which are constructed from the superposition of the exact diagonalization solutions, are very similar to charge densities obtained by the unrestricted Hartree-Fock method, e.g., compare Fig. 27 with Fig. 13 of Ref. 38.

The present finding provides an insight into the problem of the magic angular momenta.[2,3,20–22] A linear combination of any pair of states with different angular momenta produces a broken-symmetry charge density. The exceptional feature of the states with adjacent magic angular momenta is that their superposition reproduces the semiclassical charge density, which at the infinite magnetic-field limit tends to one of the degenerate classical point-charge distributions. It is obvious that any charge distribution, including the semiclassical one, can be reproduced by a superposition of angular-momentum eigenstates, since they form a complete basis. However, a superposition of more than two states would never give an exact value of the ground-state energy, since the ground state in spin-polarized circular dots is at most twofold degenerate. The subsequent magic angular momenta correspond to states which exhibit ground-state level crossing (each of the crossing levels corresponds to the ground state at its side of the level crossing). The level crossings allow the semiclassical laboratory-frame charge distribution to appear as a realizable feature of the exact ground state at the magnetic field corresponding to the crossing. We have to note here that this conclusion has been reached for systems containing a small number of electrons and we cannot exclude a different behavior for larger N.

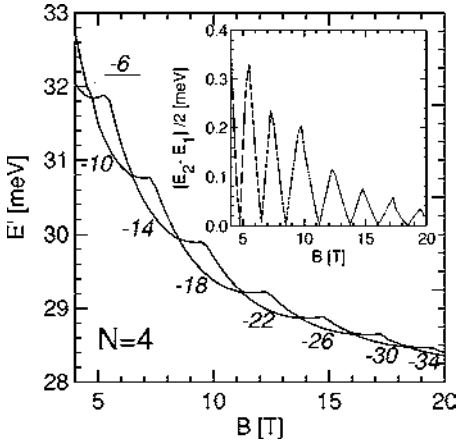

FIG. 28. Same as Fig. 24 but for $N=4$.

Mean-field approaches predict spontaneous breaking[3] of the symmetry of the confinement potential symmetry of the electron wave function after the MDD decay. Although, this effect is a notorious artifact,[3] it is generally believed that there is some deeper physics behind it. The exact solutions show a rapid increase of the electron-electron correlation after the MDD breakdown. This increase appears in the inner coordinates and can be observed in the PCF plots (cf. Figs. 11, 12, and Ref. 30). Since the mean-field theories cannot give a complete description of the inner-coordinate space, they tend to account for the electron-electron correlation in the external (laboratory) frame of reference, which results in the symmetry breaking.

The energy overestimates obtained with the broken-symmetry solutions exhibit oscillations with amplitude decreasing with the magnetic field. The precision of the ground-state energy estimates obtained by the HF wave function with semiclassical localization[24] also possesses an oscillatory dependence on the magnetic field with minima at the magnetic field corresponding to the exact ground-state transformations. Contrary to the broken-symmetry solutions obtained in the present paper at the exact-diagonalization level the HF energy overestimates take on nonzero values at their

minima.[24] The present paper shows that the fact that the HF broken-symmetry solutions overestimate the exact ground-state energy at the fields inducing its transformations is not due to their broken symmetry, but to their mean-field character. The broken-symmetry states constructed from the degenerate exact solutions presented in this paper contain a complete description of the inner-coordinate space. Due to this fact they provide the exact ground-state energy for finite values of the magnetic fields corresponding to the ground-state transformations. The HF broken-symmetry solutions account for the separation of the electron charges but the rest of the correlation effects, most probably the reaction of an electron on the actual positions of the electrons inside the other charge puddles, is missed. This missing part of the correlation is squeezed to zero in the infinite magnetic field for which the charge puddles shrink to point-charge distributions.[24]

VII. SUMMARY AND CONCLUSIONS

We presented a detailed study of the magnetic-field-induced Wigner crystallization of the two-, three-, and four-electron spin-polarized systems in quantum dots. The obtained results, although limited to small numbers of electrons, cover several symmetries of the confinement potential. We studied quantum dots of elliptical, square, triangular, and circular symmetry. In the present study, we developed a configuration-interaction scheme which was based on single-electron wave functions expanded in a multicenter basis. The method, verified for the well-known case of an isotropic harmonic-oscillator potential, can be applied to the case of any smooth confinement potential with arbitrary symmetry. The arbitrariness in the choice of centers in basis (3) allows us to achieve a high accuracy and flexibility of the present MCI method accompanied with its relatively simple applicability to low-symmetry nanostructures.

We have studied the parity transformations in the spin-polarized electron systems confined in elliptical quantum dots and found anticrossings between the energy levels of the same spatial symmetry. The experimental identification[39,40] of the magnetic-field-induced ground-state transformations for the N-electron system in a cylindrical quantum dot is based on detection of cusps of the chemical potential, i.e., the difference of the ground-state energy of the N and $N-1$ electron system. Based on the present results we expect that the ellipsoidal deformation of the quantum dot potential results in a smoothening of the cusps of the charging lines[41] corresponding to the ground-state transformations between states of the same spin and parity symmetry. On the other hand, cusps related to spin or parity transformations should remain sharp.

Quantum Wigner molecules in anisotropic quantum dots are related with the lowest-energy configurations of their classical counterparts. At high magnetic fields the quantum charge density tends to simultaneously reproduce all the degenerate lowest-energy classical configurations. Classical degeneracy occurs when the lowest-energy configuration is of a different symmetry than the confinement potential. We found that the quantum charge density is a superposition of all these degenerate classical configurations. Consequently, the quantum-mechanical charge-density reproduces the symmetry of the confinement potential. We conclude that the observation of Wigner crystallization through its charge-density distribution will be facilitated in low-symmetry quantum dots for which the symmetry of the classical configuration conforms with the symmetry of the external potential, i.e., in systems which do not exhibit classical degeneracy.

Moreover, we have found a relation between the occurrence of the magnetic-field-induced level crossings and classical degeneracy. None of the studied quantum systems with nondegenerate classical counterpart exhibit such crossings. The formation of Wigner phase in these systems is a continuous process. For majority of the studied quantum systems with degenerate classical counterparts these crossings are observed. The only exception is the four-electron system for elliptical dots for which the classical configuration has a zigzag form. We have shown that in the presence of the crossings a superposition of the two lowest-energy states produces a broken-symmetry state whose charge density reproduces one of the degenerate classical configurations. These broken-symmetry states are exact ground states for the magnetic fields for which the crossings appear and for which the ground state is twofold degenerate. The ground-state degeneracy allows the semiclassical broken-symmetry charge distribution to be a realizable property of the quantum system. This conclusion holds also for circular dots. The superposition of the adjacent magic-angular-momenta states allows the inner symmetry of the quantum system to appear in the laboratory frame of reference.

ACKNOWLEDGMENTS

This paper has been partly supported by the Polish Ministry of Scientific Research and Information Technology in the framework of the solicited grant PBZ-MIN-008/P03/2003, the Flemish Science Foundation (FWO-Vl), the Concerted Action program (IUAP), and the University of Antwerpen (VIS and GOA). One of us (B.S.) was supported by the Foundation for Polish Science (FNP).

[1] L. Jacak, P. Hawrylak, and A. Wójs, *Quantum Dots* (Springer, Berlin, 1998).

[2] P.A. Maksym, H. Immamura, G.P. Mallon, and H. Aoki, J. Phys.: Condens. Matter **12**, R299 (2000).

[3] S.M. Reimann and M. Manninen, Rev. Mod. Phys. **74**, 1283 (2002).

[4] A. Matulis and F.M. Peeters, Solid State Commun. **117**, 655 (2001).

[5] V.M. Bedanov and F.M. Peeters, Phys. Rev. B **49**, 2667 (1994).

[6] E.E. Vdovin, A. Levin, A. Patanè, L. Eaves, P.C. Main, N.Yu. Khanin, Yu.V. Dubrovkii, M. Henini, and G. Hill, Science **290**, 122 (2000).

[7] T. Ezaki, N. Mori, and C. Hamaguchi, Phys. Rev. B **56**, 6428 (1997).
[8] M. Manninen, M. Koskinen, S.M. Reimann, and B. Mottelson, Eur. Phys. J. D **16**, 381 (2001).
[9] C.E. Creffield, W. Häusler, J.H. Jefferson, and S. Sarkar, Phys. Rev. B **59**, 10 719 (1999).
[10] P.S. Drouvelis, P. Schmelcher, and F.K. Diakonos, Europhys. Lett. **64**, 232 (2003).
[11] E. Räsänen, H. Saarikoski, M.J. Puska, and R.M. Nieminen, Phys. Rev. B **67**, 035326 (2003).
[12] S. Akbar and I.-L. Lee, Phys. Rev. B **63**, 165301 (2001).
[13] D.G. Austing, S. Sasaki, S. Tarucha, S.M. Reimann, M. Koskinen, and M. Manninen, Phys. Rev. B **60**, 11 514 (1999).
[14] E. Räsänen, H. Saarikoski, V.N. Stavrou, A. Harju, M.J. Puska, and R.M. Nieminen, Phys. Rev. B **67**, 235307 (2003).
[15] A. Natori, Y. Sugimoto, and M. Fujito, Jpn. J. Appl. Phys., Part 1 **36**, 3960 (1997).
[16] B. Reusch and R. Egger, Europhys. Lett. **64**, 84 (2003).
[17] A.D. Güçlü, J.-S. Wang, and H. Guo, Phys. Rev. B **68**, 035304 (2003).
[18] L. Cândido, J.-P. Rino, N. Studart, and F.M. Peeters, J. Phys.: Condens. Matter **10**, 11 627 (1998).
[19] A.H. MacDonald, S.R.E. Yang, and M.D. Johnson, Aust. J. Phys. **46**, 345 (1993).
[20] S.M. Girvin and T. Jach, Phys. Rev. B **28**, 4506 (1983).
[21] P.A. Maksym, Phys. Rev. B **53**, 10 871 (1996).
[22] C.G. Bao, W.Y. Ruan, and Y.Y. Liu, Phys. Rev. B **53**, 10 820 (1996).
[23] C. Yannouleas and U. Landman, Phys. Rev. B **66**, 115315 (2002); **68**, 035326 (2003).
[24] B. Szafran, S. Bednarek, J. Adamowski, M.B. Tavernier, E. Anisimovas, and F.M. Peeters, Eur. Phys. J. D **28**, 373 (2004).
[25] K. Maki and X. Zotos, Phys. Rev. B **28**, 4349 (1983).
[26] R. Price, X. Zhu, S. Das Sarma, and P.M. Platzman, Phys. Rev. B **51**, 2017 (1995).
[27] M. Polini, M.K. Moulopolous, B. Davoudi, and M.P. Tosi, Phys. Rev. B **65**, 165306 (2002).
[28] J. Kainz, S.A. Mikhailov, A. Wensauer, and U. Rössler, Phys. Rev. B **65**, 115305 (2002).
[29] B. Szafran, S. Bednarek, and J. Adamowski, Phys. Rev. B **67**, 045311 (2003); J. Phys.: Condens. Matter **15**, 4189 (2003).
[30] M.B. Tavernier, E. Anisimovas, F.M. Peeters, B. Szafran, J. Adamowski, and S. Bednarek, Phys. Rev. B **68**, 115310 (2003).
[31] K. Jauregui, W. Häusler, and B. Kramer, Europhys. Lett. **24**, 581 (1993).
[32] F.M. Peeters, Phys. Rev. B **42**, 1486 (1990).
[33] S.R.E. Yang and A.H. MacDonald, Phys. Rev. B **66**, 041304 (2002).
[34] This is similar to the equivalent system of vortices in superconducting mesoscopic squares. See, e.g., B.J. Baelus and F.M. Peeters, Phys. Rev. B **65**, 104515 (2002).
[35] L.F. Chibotaru, A. Ceulemans, M. Lorenzini, and V.V. Moshchalkov, Europhys. Lett. **63**, 159 (2003).
[36] The $\pi/2$ rotation is not an observable and the average value of its operator is gauge dependent.
[37] Although in the plots in Figs. 25, 28, and 29 Wigner molecules are pinned at a similar orientation small angular differences can be noticed [e.g., the cross formed of the position of electrons in Fig. 29(a) is slightly tilted to left and in Fig. 29(b) to right]. We left these differences uncorrected to show that the positions of the charge maxima do not coincide with the position of centers, fixed at the same angles in all these plots.
[38] B. Reusch and H. Grabert, Phys. Rev. B **68**, 045309 (2003).
[39] S. Tarucha, D.G. Austing, T. Honda, R.J. van der Hage, and L.P. Kouwenhoven, Phys. Rev. Lett. **77**, 3613 (1996).
[40] B.T. Miller, W. Hansen, S. Manus, R.J. Luyken, A. Lorke, J.P. Kotthaus, S. Huant, G. Medeiros-Ribeiro, and P.M. Petroff, Phys. Rev. B **56**, 6764 (1997).
[41] B. Szafran, S. Bednarek, and J. Adamowski, Phys. Rev. B **61**, 1971 (2000); **65**, 035316 (2002); **67**, 115323 (2003).

Available online at www.sciencedirect.com
SCIENCE DIRECT®
Physica E 26 (2005) 252–256
PHYSICA E
www.elsevier.com/locate/physe

Exact broken-symmetry states and Hartree–Fock solutions for quantum dots at high magnetic fields

B. Szafran[a,b,*], F.M. Peeters[a], S. Bednarek[b], J. Adamowski[b]

[a]*Departement Natuurkunde, Universiteit Antwerpen, Campus Drie Eiken, B-2610 Antwerpen, Belgium*
[b]*Faculty of Physics and Nuclear Techniques, AGH University of Science and Technology, Kraków, Poland*

Available online 24 November 2004

Abstract

Wigner molecules formed at high magnetic fields in circular and elliptic quantum dots are studied by exact diagonalization (ED) and unrestricted Hartree–Fock (UHF) methods with multicenter basis of displaced lowest Landau level wave functions. The broken symmetry states with semi-classical charge density constructed from superpositions of the ED solutions are compared to the UHF results. UHF overlooks the dependence of the few-electron wave functions on the actual relative positions of electrons localized in different charge puddles and partially compensates for this neglect by an exaggerated separation of charge islands which are more strongly localized than in the exact broken-symmetry states.

PACS: 73.21.La; 73.20.Qt

Keywords: Quantum dots; Wigner molecules

At high magnetic fields the electron systems in circular quantum dots form Wigner molecules [1,2] in the internal structure of the system. Deformation [3,4] of the circular symmetry allows the molecules to appear in the laboratory frame only [4] when the classical counterpart [5] of the quantum system possesses a single lowest-energy configuration. Otherwise the charge density at high field is a superposition of equivalent semi-classical densities and the quantum system undergoes symmetry transformations when the magnetic field is increased [4]. These transformations are associated with level crossings at which the ground state is two-fold degenerate. Superposition of the states of the degenerate levels allows [4] to extract the semi-classical broken-symmetry charge density into the laboratory frame. On the other hand, the unrestricted Hartree–Fock (UHF) produces [1] broken-symmetry states for Wigner molecules. In

*Corresponding author. Universiteit Antwerpen, Campus Drie Eiken, Departement Natuurkunde, Antwerpen 2610, Belgium.
E-mail address: bartlomiej.szafran@ua.ac.be (B. Szafran).

1386-9477/$ - see front matter © 2004 Elsevier B.V. All rights reserved.
doi:10.1016/j.physe.2004.08.059

the infinite magnetic field limit UHF gives exact [6] results for the total energy. At finite magnetic fields for which exact broken-symmetry eigenstates exist the artifactal symmetry breaking cannot be blamed for the inaccuracy of the UHF [4]. In this paper, we look for the effects neglected by UHF comparing the ED and UHF solutions for elliptical and circular dots.

We assume a spin-polarization of electrons at high magnetic field $(0, 0, B)$ oriented perpendicular to the quantum dot plane and use the Landau gauge. In the ED, described in detail in Ref. [4], the single electron wave functions used for construction of the Slater determinants are obtained via diagonalization of the single electron Hamiltonian in the multicenter basis [7–9] of M-displaced lowest Landau level wave functions

$$\psi(\mathbf{r}) = \sum_{k=1}^{M} c_k \exp\{-\alpha[(x-x_k)^2 + (y-y_k)^2]/4 + \mathrm{i}eB(x-x_k)(y+y_k)/2\hbar\}, \quad (1)$$

where α is treated as a variational parameter. In the present UHF approach one-electron orbitals (1) are optimized self-consistently. We study up to $N = 4$ electrons, use the material data of GaAs and a basis of 12 centers (x_k, y_k) put on an ellipse with a size determined variationally. The basis (1) of displaced lowest Landau level wave functions reproduces [4] also higher Fock–Darwin bands. Contrary to previous multicenter HF calculations [6,9] using a single center per electron, the present HF approach produces results which are exact in the UHF [10] sense.

Classical system of three electrons in an elliptical confinement potential with $\hbar\omega_x = 3\,\mathrm{meV}$ and $\hbar\omega_y = 4\,\mathrm{meV}$ possesses two equivalent lowest-energy configurations (cf. inset of Fig. 1) and the quantum system undergoes parity transformations [4] with the magnetic field (cf. Fig. 1). Superposition [4] of the two lowest-energy eigenstates

$$\Psi_{\mathrm{BS}} = (\Psi_{\mathrm{even}} + \mathrm{e}^{\mathrm{i}\phi}\Psi_{\mathrm{odd}})/\sqrt{2} \quad (2)$$

yields a broken-symmetry (BS) charge density with a distinct electron separation. Fig. 1 shows that in contrast to the exact ground-state energy the UHF energy estimate is a smooth function of the magnetic field.

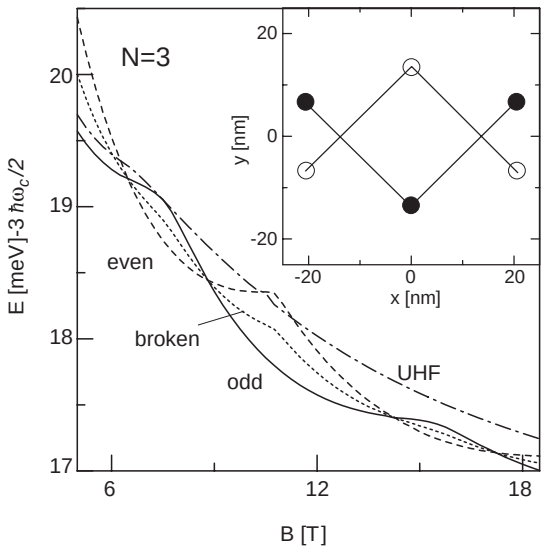

Fig. 1. Energy of the lowest even (dashed curve) and odd parity (solid curve) levels, the broken symmetry state (dotted curve) and UHF energy calculated for $N = 3$, $\hbar\omega_x = 3\,\mathrm{meV}$ and $\hbar\omega_y = 4\,\mathrm{meV}$. Inset shows the two equivalent classical configurations.

The charge densities of considered states are shown in Figs. 2(a) and (b) for two magnetic field values corresponding to the even–odd energy crossing presented in Fig. 1. The phase ϕ in the BS state is chosen such that the electrons are localized at the classical Wigner molecule positions. Notice that in the UHF the separation of electrons is more pronounced than in the exact BS states. Fig. 2(c) shows the pair correlation function (PCF) [2] for the UHF and the exact BS state corresponding to the charge density of Fig. 2(a) with the position of one of the electrons fixed at two different locations: in the center and on the edge of the central charge puddle. In contrast to the exact BS state in the UHF wave function two electrons are insensitive to the actual position of the third electron in its charge puddle. This is a consequence of the single-determinantal form of the UHF wave function, and can be easily explained for two electrons. In the spin-polarized two electron Wigner molecule the UHF spatial wave function is given by $\Psi_\alpha(\mathbf{r}_1)\Psi_\beta(\mathbf{r}_2) - \Psi_\beta(\mathbf{r}_1)\Psi_\alpha(\mathbf{r}_2)$, where $|\Psi_\alpha|^2$ and $|\Psi_\beta|^2$ are the charge densities of separate charge puddles α and β. Wave functions Ψ_α and Ψ_β are orthogonal due to the

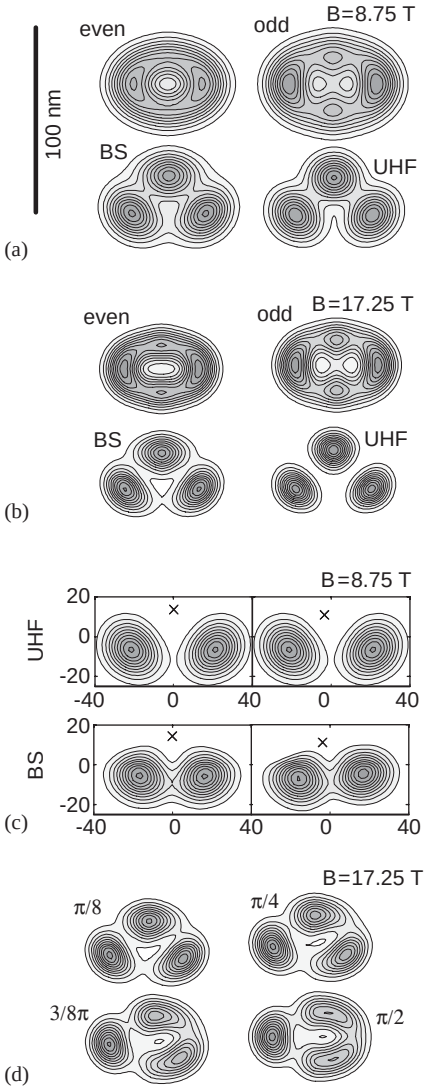

Fig. 2. (a) The charge densities for the even, the odd, the broken-symmetry (BS) state and the UHF for $N=3$, $\hbar\omega_x=3\,\mathrm{meV}$, $\hbar\omega_y=4\,\mathrm{meV}$ at $B=8.75\,\mathrm{T}$. (b) Same as (a) at $B=17.25\,\mathrm{T}$. (c) Pair correlation function plots for UHF and BS state for an electron fixed at (0,13.4 nm) (left panel) and (-3 nm,10.4 nm) [right panel] marked by crosses. (d) BS states for given shifts of phase ϕ (Eq. (2)) with respect to the BS plot in (b). Plots (a), (b) and (d) have the same scale given by the length bar in (a).

vanishing overlap between the puddles. The calculation of the PCF gives (up to a constant) $\mathrm{PCF}=|\Psi_\alpha(\mathbf{r}_a)|^2|\Psi_\beta(\mathbf{r}_b)|^2+|\Psi_\alpha(\mathbf{r}_b)|^2|\Psi_\beta(\mathbf{r}_a)|^2$. For $\mathbf{r}_b$ inside puddle β the second term of the sum vanishes and the remaining one signifies that the probability of finding an electron in point $\mathbf{r}_a$ inside puddle α is independent of the actual position of the second electron in puddle β.

The UHF self-consistency is reached only in one of the two classical orientations (cf. inset of Fig. 1) in which the UHF energy is minimal. On the other hand, the exact BS states can be oriented under an arbitrary angle (cf. Fig. 2(d)) by modifying the phase ϕ in Eq. (2). Moreover, since the BS state is constructed with states of opposite parities, all the plots in Fig. 2(d) correspond to the same value of the kinetic, potential and electron–electron interaction energies equal to the arithmetic average of the expectation values for Ψ_{odd} and Ψ_{even} states.

Fig. 3 shows the two lowest energy levels and the UHF total energy calculated with respect to the lowest Landau level for the elliptical dot with $\hbar\omega_x=3\,\mathrm{meV}$ and $\hbar\omega_y=4\,\mathrm{meV}$. For these values the classical counterpart of the four-electron system is unique and conform with the symmetry of the confinement potential, so that the Wigner crystallization is visible in the exact quantum ground-state for an arbitrary magnetic field after the MDD decay. In this case, the MDD decay is a

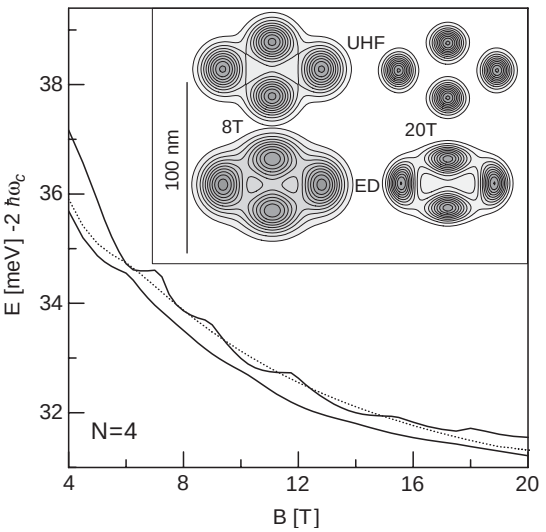

Fig. 3. Lowest energy levels for $N=4$, $\hbar\omega_x=3\,\mathrm{meV}$ and $\hbar\omega_y=4\,\mathrm{meV}$ (solid lines) and total UHF energy (dotted) line. Inset: Charge density calculated in the UHF (two upper plots) and the ED (two lower plots) for $B=8\,\mathrm{T}$ (left side) and $B=20\,\mathrm{T}$ (right side).

continuous process and appears at the anticrossing around 6 T.

The inset to Fig. 3 shows the charge densities calculated with the UHF and ED methods. In ED the charge density in between the charge maxima takes on larger values than in UHF in which the separation of electrons is more distinct.

The average radius of the charge puddle as obtained for the two-electron ground state in the circular quantum dot ($\hbar\omega_x = \hbar\omega_y = 3\,\mathrm{meV}$) is displayed in Fig. 4. The ED and UHF values are similar below the MDD breakdown ($B < 5.6\,\mathrm{T}$). The exact value has discontinuities at the angular momentum transitions. After the MDD decay the UHF value is close to the average around which ED and BS results oscillate, but at higher fields it becomes an upper bound for these oscillations. The inset of Fig. 4 shows the exact BS and UHF charge density for $B = 11.8$ and 28.9 T. BS charge densities for the two values of the magnetic field have been obtained from superpositions of the degenerate states with angular momenta $-5, -7$ and $-9, -11$ (in $\hbar$ units), respectively. The charge

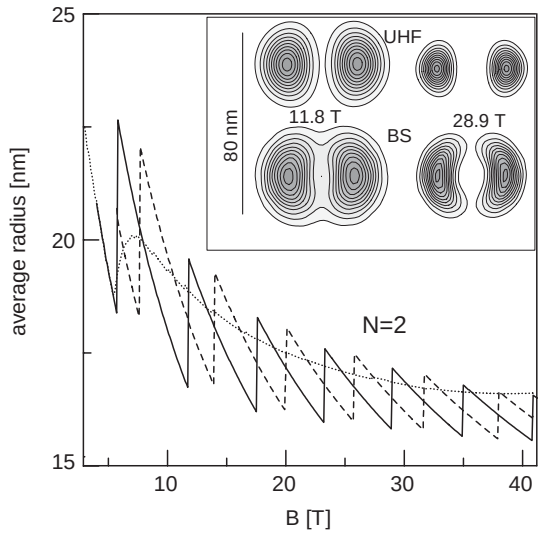

Fig. 4. Average radius of the charge puddle $[(<\mathbf{r}_1^2 + \mathbf{r}_2^2>/2)^{1/2}]$ for two electrons in a circular quantum dot ($\hbar\omega_x = \hbar\omega_y = 3\,\mathrm{meV}$). Dotted, dashed and solid lines correspond to UHF, BS, and ED results. Inset: charge density obtained in the UHF (two upper plots) and in the exact broken-symmetry state (two lower plots) for B = 11.8 T (left side) and 28.9 T (right side).

maxima in the exact BS solutions are less strongly separated. For $B = 28.9\,\mathrm{T}$ the charge density islands of the exact BS have a crescent shape while the UHF charge puddles are more oval and the distance between them is larger.

The difference in shape of the separated charge islands in circular dots is largest for $N = 2$. For larger N the charge puddles in the exact solutions are less spectacularly spread. Fig. 5 shows the comparison of the exact BS and UHF charge densities for $N = 3$. The BS plots for $N = 3$ correspond to degeneracy of states with angular momentum $-9\hbar$, $-12\hbar$ for $B = 7.5\,\mathrm{T}$ and $-12\hbar, -15\hbar$ for $B = 15\,\mathrm{T}$.

In summary, we have presented a comparison of the UHF and the ED results for the charge density of Wigner molecules in circular and elliptical dots. For the comparison we have used the broken-symmetry states obtained from the superposition of the exact eigenstates. We have found that the UHF exaggerates the separation of the electron charge densities in the laboratory frame. In this way, the UHF method partially compensates for the overlooked correlations related to the reaction of electrons on their actual position in the separated charge density islands. This reaction is of smaller importance for larger magnetic fields, for which the charge density islands shrink to points, which explains the vanishing of the UHF energy overestimation in the infinite magnetic field [6]. Due to the exaggerated electron separation the charge islands forming Wigner molecules calculated in the UHF shrink with the magnetic field faster than in the exact broken-symmetry states.

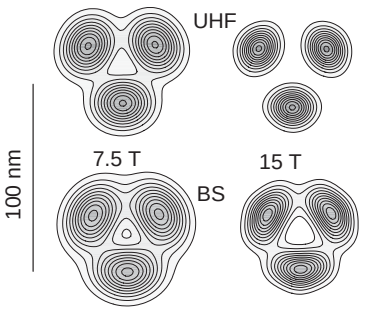

Fig. 5. Charge density for $N = 3$ electrons in a circular quantum dot ($\hbar\omega_x = \hbar\omega_y = 3\,\mathrm{meV}$) calculated with UHF (upper plots) and for exact BS states (lower plots) for $B = 7.5\,\mathrm{T}$ (left plots) and $B = 15\,\mathrm{T}$ (right plots).

Acknowledgements

This paper was supported in part by the Polish Ministry of Scientific Research and Information Technology in the framework of the solicited Grant PBZ-MIN-008/P03/2003, the Flemish Science Foundation (FWO-Vl), the Belgian Science Policy, and the University of Antwerpen (VIS and GOA). One of us (BS) is supported by the Foundation for Polish Science (FNP).

References

[1] S.M. Reimann, M. Manninen, Rev. Mod. Phys. 74 (2002) 1283.
[2] P.A. Maksym, H. Immamura, G.P. Mallon, H. Aoki, J. Phys. Condens. Matt. 12 (2000) R299.
[3] M. Manninen, M. Koskinen, S.M. Reimann, B. Mottelson, Eur. Phys. J. D 16 (2001) 381.
[4] B. Szafran, F.M. Peeters, S. Bednarek, J. Adamowski, Phys. Rev. B 69 (2004) 125344.
[5] V.M. Bedanov, F.M. Peeters, Phys. Rev. B 49 (1994) 2667.
[6] B. Szafran, S. Bednarek, J. Adamowski, M. Tavernier, E. Anisimovas, F.M. Peeters, Eur. Phys. J. D 28 (2004) 373.
[7] J. Kainz, S.A. Mikhailov, A. Wensauer, U. Rössler, Phys. Rev. B 65 (2002) 115305.
[8] C. Yannouleas, U. Landman, Phys. Rev. B 66 (2002) 115315.
[9] B. Szafran, S. Bednarek, J. Adamowski, Phys. Rev. B 67 (2003) 045311;
B. Szafran, S. Bednarek, J. Adamowski, J. Phys.: Condens. Matter 15 (2003) 4189.
[10] B. Reusch, H. Grabert, Phys. Rev. B 68 (2003) 045309.

EUROPHYSICS LETTERS 1 June 2004

Europhys. Lett., **66** (5), pp. 701–707 (2004)
DOI: 10.1209/epl/i2003-10250-8

Re-entrant pinning of Wigner molecules in a magnetic field due to a Coulomb impurity

B. Szafran[1,2] and F. M. Peeters[1]

[1] *Departement Natuurkunde, Universiteit Antwerpen (Campus Drie Eiken) B-2610 Antwerpen, Belgium*
[2] *Faculty of Physics and Nuclear Techniques, AGH University of Science and Technology - al. Mickiewicza 30, 30-059 Kraków, Poland*

(received 5 December 2003; accepted in final form 29 March 2004)

PACS. 73.21.La – Quantum dots.
PACS. 73.20.Qt – Electron solids.

Abstract. – Pinning of magnetic-field–induced Wigner molecules (WMs) confined in parabolic two-dimensional quantum dots by a charged defect is studied by an exact diagonalization approach. We found a re-entrant pinning of the WMs as a function of the magnetic field, a magnetic-field–induced re-orientation of the WMs and a qualitatively different pinning behaviour in the presence of a positive and negative Coulomb impurity.

Low-density electron systems in bulk may form an ordered crystalline phase called Wigner crystal [1] in which electron charges are spatially separated. A similar collective type of electron localization in quantum dots (QDs) is called Wigner molecule (WM) [2]. WMs may be formed in large QDs [2] or be induced by a strong magnetic field [3] in the quantum Hall regime. Wigner localization is observed in the inner coordinates of the quantum system whose charge density conserves the symmetry of the external potential [4]. Therefore, in circular QDs [4, 5] the charge density will be circular symmetric even in the Wigner phase. However, a perturbation of the potential may pin [6] the charge density at a fixed orientation in the laboratory frame which should allow for the experimental observation [7] of Wigner localization. Pinning of the magnetic-field–induced WMs by the anisotropy of the potential [8] or by an attractive Gaussian impurity potential [9] in the absence of a magnetic field have been studied previously. Here, we will show that the WM pinning is qualitatively very different in the presence of a positive and negative impurity.

We consider WMs induced by a magnetic field in a two-dimensional harmonic QD. A strong magnetic field polarizes the spins of the confined electrons and leads to the formation of a so-called maximum density droplet (MDD) corresponding to the lowest Landau level filling factor $\nu = 1$. Stronger fields induce the MDD to decay into a molecular phase with $\nu < 1$, for which the distribution of electrons in the inner coordinates resembles the equilibrium configuration of a classical point-charge system [10]. The external magnetic field increases the absolute value of the angular momentum of the confined electron system inducing its changes

between certain "magic" [11] values for which the classical distribution of electrons in the inner ("rotating") frame of reference can be realized.

In this letter we investigate the way in which the potential of a charged defect (donor or acceptor ion) situated outside the QD symmetry axis stops the "rotation" of the electron system and freezes the WM at a fixed orientation. We use the configuration interaction approach which allows for an exact solution of the few-electron Schrödinger equation. We found that at magnetic fields inducing the angular-momentum transitions the exact ground state can correspond to broken-symmetry charge density with semi-classical localization in the laboratory frame. Broken-symmetry charge distributions were previously obtained as artifacts of mean-field methods [4]. The existence of exact broken-symmetry states makes the WMs susceptible to pinning by an arbitrarily distant charge defect (donor or acceptor ion) at the angular-momentum transitions. Consequently, a distant defect induces re-entrant WM pinning as a function of the strength of the magnetic field. We show that the orientation of the pinned WMs can change with the magnetic field and demonstrate an essentially different pinning behavior for a positive and negative impurity.

We assume that the system of N electrons is spin-polarized by the external magnetic field and that the electrons are confined to move in the $z = 0$ plane. The present configuration interaction approach is constructed in the following way. The single-electron Hamiltonian for the considered system reads

$$h = (-i\hbar\nabla + e\boldsymbol{A})^2/2m^* + m^*\omega^2\big(x^2 + y^2\big)/2 + Bs_z g^*\mu_{\mathrm{B}} \pm e^2/4\pi\epsilon\epsilon_0 r_{\mathrm{ed}}\,, \tag{1}$$

where m^* is the electron band effective mass, $\hbar\omega$ is the confinement potential energy, ϵ_0 is the static dielectric constant, $(0, 0, B)$ is the magnetic-field vector, s_z is the z-component of the electron spin, g^* is the effective Landé factor and r_{ed} is the distance between the electron and the charged defect. The sign in the last term of eq. (1) is $-$ $(+)$ for a positively (negatively) charged defect. We apply the Landau gauge $\boldsymbol{A} = (-By, 0, 0)$ and adopt GaAs material parameters $m^* = 0.067m_0$, $\epsilon = 12.9$ and $g^* = -0.44$ as well as $\hbar\omega = 3\,\mathrm{meV}$. Hamiltonian (1) is diagonalized in a multicenter basis $\Psi_\mu(\boldsymbol{r}) = \sum_{i=1}^{M} c_i^\mu \psi_{\boldsymbol{R}_i}(\boldsymbol{r})$ with

$$\psi_{\boldsymbol{R}}(\boldsymbol{r}) = \sqrt{\alpha}\exp\big[-\alpha(\boldsymbol{r} - \boldsymbol{R})^2/4 + ieB(x - X)(y + Y)/2\hbar\big]/\sqrt{2\pi}, \tag{2}$$

where $\boldsymbol{R} = (X, Y)$. The single-electron wave functions Ψ_μ are subsequently used for the construction of $M!/N!(M - N)!$ Slater determinants —the basis set for diagonalization of the N-electron Hamiltonian. α and the positions of the centers $\boldsymbol{R}_i$ are chosen such that they minimize the total energy. Function (2) with $\alpha = eB/\hbar$ is the lowest Landau level eigenfunction. The basis set of displaced functions (2) allows for a very precise determination of the exact Fock-Darwin [4] energy levels, including higher Fock-Darwin bands, which at strong magnetic fields tend to excited Landau levels. We have verified the accuracy of the present approach comparing its results with the standard exact diagonalization method [12]. We have taken 12 centers placed on a circle. Above the MDD decay ($B > 5.8$, 4.85 and 4.65 T for 2, 3 and 4 electrons) and below 20 T, the overestimation of the exact energy for 2, 3 and 4 electrons is lower than 0.01, 0.06 and 0.12 meV, respectively. Few-electron wave functions calculated in the Landau gauge are not eigenfunctions of the angular momentum, but using the gauge-independent expectation value of its operator we can look at the angular-momentum transformations of the confined system. The precision in the determination of the critical fields inducing ground-state transformation is better than 0.15 T. Previously, displaced Landau level functions (2) were used in the investigation of the WMs with approximate approaches, *i.e.*, single-determinant of non-orthogonal wave functions [13], Hartree-Fock [14],

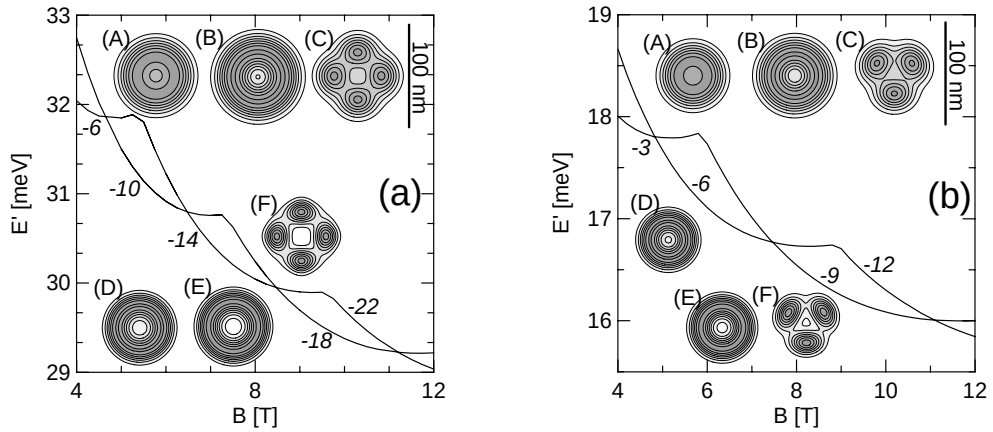

Fig. 1 – (a) Two lowest-energy levels of the 4-electron unperturbed circular QD calculated with respect to the lowest Landau level. Numbers denote L - angular momentum in $\hbar$ units. Insets (A), (B) and (C) display the charge densities of the states for $B = 4.6\,\mathrm{T}$ corresponding to $L = -6$, -10 and broken symmetry, respectively (the darker the shade of grey the larger the density). (D), (E) and (F) show the charge density of the degenerate states with $L = -18$, -22 and broken symmetry for $B = 11.2\,\mathrm{T}$. (b) Same as (a) but for 3 electrons. (A), (B) and (C) plotted for $B = 4.2\,\mathrm{T}$ correspond to $L = -3$, -6 and broken symmetry, respectively. (D), (E) and (F) show the charge density of degenerate states with $L = -9$, -12 and broken symmetry for $B = 11.2\,\mathrm{T}$.

and rotated-electron-molecule approach [15]. Due to the arbitrariness in the choice of centers the present configuration interaction approach can be easily applied to potentials without circular symmetry. In the calculations for the perturbed QDs, we used 12 centers placed on an ellipse, the size and its center of gravity were optimized variationally.

Figure 1 shows the two lowest 4- (a) and 3- (b) electron energy levels calculated with respect to the lowest Landau level ($E' = E - N \times 0.85\,(\mathrm{meV/T})$) as functions of the magnetic field. E' at high field tends to the potential energy of a classical point charge system [13]. At lower magnetic fields, the ground state is the MDD with angular momentum $-N(N-1)\hbar/2$. At larger magnetic fields, the angular momentum decreases by $N\hbar$ [4,5,11]. The ground-state charge density after the MDD decay has a ring-like shape with a pronounced minimum at the center of the dot. At each ground-state transformation, the central local minimum becomes wider and the size of the charge puddle exhibits a stepwise increase. Between the ground-state transformations, the magnetic field compresses the charge density which shrinks in a continuous fashion [12].

At the angular momentum transformations, the ground-state charge density is twofold degenerate. Consequently, each linear combination of the degenerate ground states Φ_1 and Φ_2 is also an eigenstate. Consider the following combination: $\Phi_{\mathrm{bs}} = (\Phi_1 + c\Phi_2)/\sqrt{2}$, with $|c|^2 = 1$. Since the angular momenta of degenerate ground states differ by $N\hbar$, the angular momentum in state Φ_{bs} is not defined and Φ_{bs} possesses a broken-symmetry charge distribution (cf. insets (C) and (F) in fig. 1). The charge density of the *exact* broken-symmetry states resembles the *approximate* mean-field broken-symmetry solutions [4]. The broken-symmetry charge distributions at high field tend [14] to the classical lowest-energy distribution of point charges [10]. Superposition Φ_{bs} extracts the inner symmetry of the magic-angular-momenta states into the laboratory frame of reference. The broken-symmetry charge distribution can be oriented at an arbitrary angle depending on the phase of c.

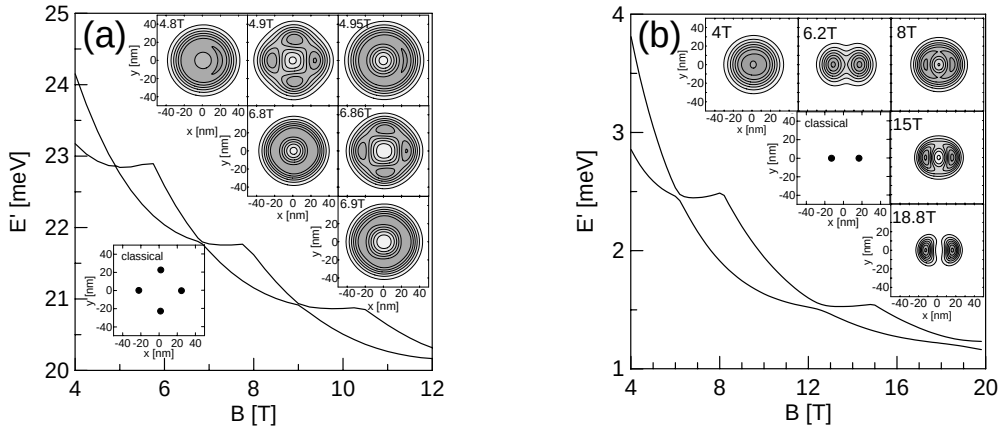

Fig. 2 – (a) Two lowest-energy levels of the 4-electron system in a circular QD perturbed by a potential of a positively charged defect situated at $(20, 0, 40)$ nm. The insets show the ground-state charge densities and the lowest-energy configuration of the classical system. (b) Same as (a) but for 2 electrons.

Let us now suppose that at a certain distance of the quantum dot plane there is an impurity ion located off the symmetry axis of the dot. In vertical quantum dots [16] for which the harmonic approximation of the potential is justified [17], and in which the MDD decay has been observed [16], ionized [17] donor impurities are present at a distance of 20–30 nm from the QD plane. The defect potential perturbs the QD circular symmetry and mixes the angular-momentum eigenstates. Level crossings are replaced by avoided crossings. Figure 2(a) shows the two lowest-energy levels and the ground-state charge density for 4 electrons with a positively charged defect situated at point $x = 20$, $y = 0$, $z = 40$ nm. The energy gaps in the avoided crossings are very small ($\sim 10^{-3}$ meV). At the avoided level crossings (see insets for $B = 4.9$ and 6.86 T) Wigner crystallization in the laboratory frame (*i.e.* WM pinning) can be observed. The positions of the pinned charge density maxima coincide with the position of classical electrons in the lowest energy configurations (cf. lowest inset of fig. 2(a)). The charge density plots for the magnetic fields outside the avoided level crossings resembles the unperturbed circular densities (cf. fig. 1(a)), although an increased density at the right end of the charge puddle is visible. Since the "momentary" pinning is a consequence of the existence of the exact broken-symmetry states, it appears for an arbitrarily far situated defect.

Figure 2(b) shows that the effect of the defect on the 2-electron spectrum and the charge density is much stronger (energy gaps are about 5×10^{-2} meV). The oscillatory character of the pinning as a function of the magnetic field is visible. At avoided level crossings separation of the electron charges is particularly pronounced (see insets for 6.2 and 18.8 T). The effect of the negatively charged defect at this rather large distance from the QD is similar, although the molecules become pinned at different angles.

The pinning effect is stronger when the defect is closer to the QD plane. In the rest of the paper we consider a defect located at $(20, 0, 20)$ nm. Figure 3 shows the results for 2 electrons. An attractive impurity (fig. 3(a)) enhances the harmonic QD potential which results in a stronger charge localization and, as a consequence, shifts the anticrossings to higher values of the magnetic field. The energy gap between the lowest levels is larger for repulsive defect (fig. 3(b)). In both systems, an anticrossing related with the MDD breakdown is visible (~ 7 T in (a) and ~ 5 T in (b)). Both systems present smooth non-oscillatory convergence to the lowest-energy configuration of their classical counterparts.

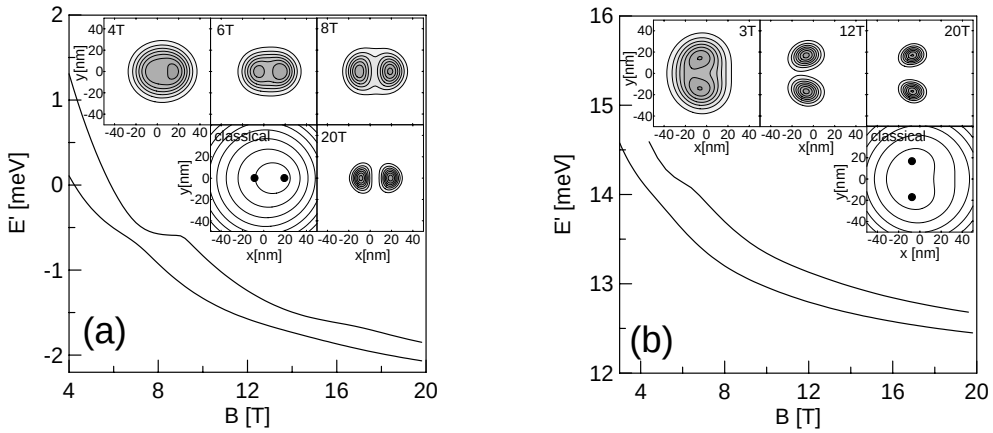

Fig. 3 – Two lowest-energy levels of the 2-electron system in a QD perturbed by (a) positively and (b) negatively charged impurity situated at $(20, 0, 20)$ nm. The insets show the ground-state charge densities as well as the classical configurations on a background of potential profile (the equipotential lines are spaced by 3 meV).

Figure 4 shows the plots for an attractive impurity with $N = 3$ (a) and $N = 4$ (b). For both $N = 3$ and 4, the energy gaps between the anticrossing levels remain small (around 0.01 meV (0.04 meV) for $N = 4$ (3)) and the pinning of the WMs exhibits anew the oscillatory dependence on the magnetic field. The distribution of charge maxima in the WMs pinned at the MDD breakdown (5.8 T for $N = 3$ and 5.3 T for $N = 4$) differs from their classical counterparts. In classical systems, a single electron is trapped under the attractive impurity. In the WM pinned at the MDD breakdown, 2 electrons fit in the local minimum of the potential induced by the defect. At higher fields (9 T for $N = 3$ and 10.15 T for $N = 4$) the pinning fixes the charge maxima near the equilibrium positions of classical electrons. Thus, an interesting rotation of the pinned WM is found as a function of the magnetic field. The

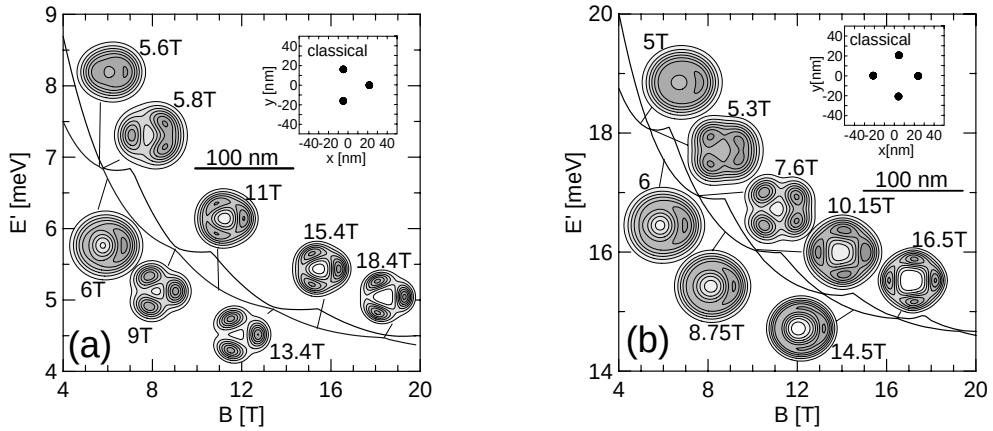

Fig. 4 – (a) Two lowest-energy levels of the 3-electron system in a QD perturbed by a positively charged defect situated at $(20, 0, 20)$ nm. The insets show the ground-state charge densities as well as the classical lowest-energy configuration. (b) Same as (a) but for 4 electrons.

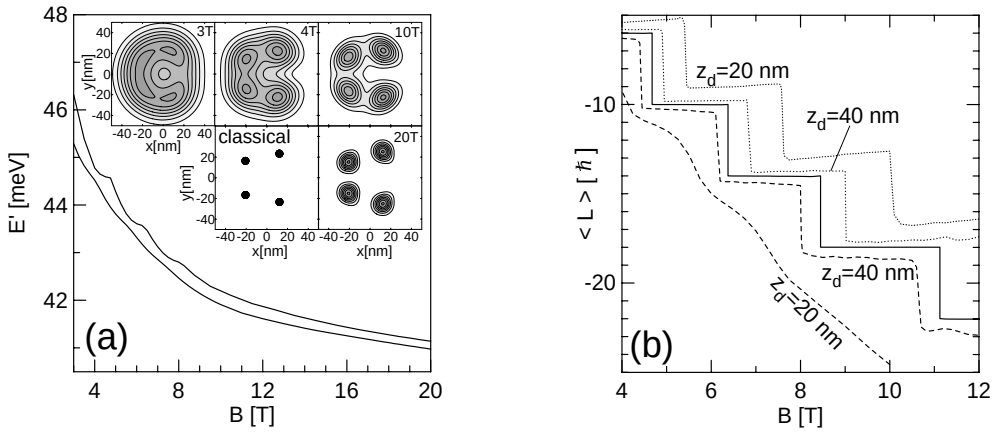

Fig. 5 – (a) Same as fig. 4(b) but for a negatively charged defect. (b) Average value of the total angular momentum for 4 electrons without the defect (solid line), in the presence of an attractive (dotted lines) and a repulsive (dashed lines) defect at $(20\,\mathrm{nm}, 0, z_d)$.

change in the charge distribution in the WMs between the MDD decay and the classical limit is similar to the magnetic-field–induced transformations of the WMs in circular dots for larger N [14]. At high magnetic field, the 3-electron charge density acquires the semi-classical charge distribution even between the anticrossings (cf. plots for 11 and 15.4 T in fig. 4(a)). This is not observed for $N = 4$ in the studied magnetic-field range.

The results for 4 electrons in the presence of a repulsive defect are shown in fig. 5. The ground-state energy is a smooth function of the magnetic field and oscillations appear only in the excited state. A continuous MDD decay appears around 4 T. The charge density tends in a non-oscillatory way to the classical limit of point charges.

The influence of the charged defects on the average value of the total angular momentum for 4 electrons is shown in fig. 5(b). In the presence of a defect, the average values of angular momentum take non-integer values and their dependence on the magnetic field becomes continuous; however, much of the stepwise character of a pure QD is conserved for the positive impurity as well as for a distant negative defect. For the positive (negative) defect, the electrons become localized closer to (further from) the origin which results in a decrease (increase) of the absolute value of the angular momentum with respect to the unperturbed case. For a negative defect closer to QD plane the average value is a smoothly decreasing function of the magnetic field. This fast increase of the absolute value of angular momentum is related to the localization of the charge density near the classical equilibrium points (cf. fig. 5). Results for 3 electrons for this position of the negative defect are qualitatively the same as for 4 electrons.

Comparing the results for an attractive with those of a repulsive defect (cf. figs. 4 and 5) shows that the pinning is much more effective in case of a repulsive defect. The attractive defect enhances the confinement potential of the QD, decreases its size and hinders the Wigner crystallization itself. Moreover, it binds one of the electrons in its neighborhood. The potential of the bound electron and the defect potential partially cancels and, as a consequence, the other electrons see a nearly circular potential and the system in the external magnetic field behaves essentially like a $N - 1$ electron system. On the other hand, the potential of the repulsive defect is not screened, so it breaks the circular symmetry of the potential felt by each of the electrons in a more pronounced manner.

In conclusion, magnetic-field–induced WMs in circular dots are from their very nature susceptible to pinning by the potential of an external charged defect at the angular-momentum transitions. Our results can be summarized as follows: 1) At large distance between the QD plane and the defect, the pinning has a re-entrant character, *i.e.*, it appears only at the energy level anticrossings, which are situated near the angular momentum transition fields of the unperturbed system. 2) For an impurity placed closer to the QD plane, the pinning by the repulsive defect is more effective and leads to a non-oscillatory convergence of the charge density to the classical limit at high field for all N. The pinning effect of a positively charged defect is strong only for two electrons. For larger numbers of electrons it is weakened by a partial screening of the defect potential by an electron trapped in the defects neighborhood so that the re-entrant pinning behaviour is conserved. 3) For a positively charged defect close to the QD, a magnetic-field–induced re-orientation of the WM is predicted.

* * *

This paper has been supported by the Polish Ministry of Scientific Research and Information Technology in the framework of the solicited grant PBZ-MIN-008/P03/2003, the Flemish Science Foundation (FWO-Vl), the Belgian Science Policy and the University of Antwerpen (VIS and GOA). One of us (BS) is supported by the Foundation for Polish Science (FNP).

REFERENCES

[1] Wigner F. P., *Phys. Rev.*, **46** (1934) 1002.
[2] Egger R., Häusler W., Mak C. H. and Grabert H., *Phys. Rev. Lett.*, **82** (1999) 3320.
[3] Müller H.-M. and Koonin S. E., *Phys. Rev. B*, **54** (1996) 14532.
[4] Reimann S. M. and Manninen M., *Rev. Mod. Phys.*, **74** (2003) 1283.
[5] Maksym P. A., Immamura H., Mallon G. P. and Aoki H., *J. Phys. Condens. Matter*, **12** (2000) R299.
[6] Pudalov V. M., D'Orio M., Kravchenko S. V. and Campbell J. W., *Phys. Rev. Lett.*, **70** (1993) 1866.
[7] Vdovin E. E., Levin A., Patanè A., Eaves L., Main P. C., Khanin N. Yu., Dubrovkii Yu. V., Henini M. and Hill G., *Science*, **290** (2000) 122.
[8] Manninen M., Koskinen M., Reimann S. M. and Mottelson B., *Eur. Phys. J. D*, **16** (2001) 381.
[9] Reusch B. and Egger R., *Europhys. Lett.*, **64** (2003) 84.
[10] Bedanov V. M. and Peeters F. M., *Phys. Rev. B*, **49** (1994) 2667.
[11] Maksym P. A., *Phys. Rev. B*, **53** (1996) 10871.
[12] Tavernier M. B., Anisimovas E., Peeters F. M., Szafran B., Adamowski J. and Bednarek S., *Phys. Rev. B*, **69** (2003) 205305.
[13] Kainz J., Mikhailov S. A., Wensauer A. and Rössler U., *Phys. Rev. B*, **65** (2002) 115305.
[14] Szafran B., Bednarek S. and Adamowski J., *Phys. Rev. B*, **67** (2003) 045311.
[15] Yannouleas C. and Landman U., *Phys. Rev. B*, **68** (2003) 035326.
[16] Oosterkamp T. H., Janssen J. W., Kouwenhoven L. P., Austing D. G., Honda T. and Tarucha S., *Phys. Rev. Lett.*, **82** (1999) 2931.
[17] Bednarek S., Szafran B. and Adamowski J., *Phys. Rev. B*, **64** (2001) 195303.

Exchange energy tuned by asymmetry in artificial molecules

B. Szafran,[1,2] F. M. Peeters,[1] and S. Bednarek[2]
[1]*Departement Fysica, Universiteit Antwerpen (Campus Drie Eiken), B-2610 Antwerpen, Belgium*
[2]*Faculty of Physics and Nuclear Techniques, AGH University of Science and Technology, al. Mickiewicza 30, 30-059 Kraków, Poland*
(Received 15 July 2004; revised manuscript received 7 September 2004; published 11 November 2004)

Laterally coupled asymmetric quantum dots occupied by two electrons are studied using the exact diagonalization approach. It is shown that the asymmetry enhances the exchange energy, i.e., the triplet-singlet energy difference for finite magnetic fields. At high magnetic field, electrons enter the deepest dot more easily if they have parallel spins.

DOI: 10.1103/PhysRevB.70.205318 PACS number(s): 73.21.La

The spins of an electron pair in coupled quantum dots[1] were proposed[2] to serve as a basis of a quantum gate for a solid-state quantum computer. The coupling between the spins can be realized in the orbital[3] degrees of freedom exploiting the spatial symmetry of the singlet and triplet wave functions. The strength of the coupling is quantified by the exchange energy defined[3] as the energy difference of the lowest triplet and the lowest singlet states. The value of the exchange energy depends on interdot tunnel coupling. In vertically stacked dots[1,4–8] the coupling is fixed by the process of the growth which determines the composition and thickness of the interdot layer. The interdot barrier can be more conveniently controlled in laterally coupled dots[1,3,9–15] by potentials applied to gate electrodes. But there are possible difficulties with the control of the exchange energy resulting from the fact that electrostatic confinement potential in gated quantum dots is usually weak.[16] In such quantum dots with weak confinement the dominant electron Coulomb repulsion leads to the formation of Wigner molecules[1] for which the ground state becomes degenerate with respect to the spin. This is due to the vanishing overlap between the single-electron wave functions.[8,17] Therefore for a pair of large quantum dots the exchange energy may remain negligibly small even if the interdot barrier is totally removed. Consequently, the exchange energy risks to be too small to be of practical use for spin control.

The exchange energy can be controlled by an external magnetic field.[3,4,7,12–14] But its value is maximal in the absence of the field.[3,4,7,12–14] The application of a magnetic field diminishes the interdot tunnel coupling due to an increased localization[18] of the electrons in each of the dots. A high magnetic field results in a large effective interdot barrier leading to a vanishing exchange energy[3] due to the separation of the single-electron wave functions. This is similar to Wigner crystallization appearing in a single large quasi-one-dimensional quantum dot.[8,17] In a single circular quantum dot the magnetic field induces singlet-triplet oscillations[1] which when the Zeeman spin effect is neglected, continue to infinity. In coupled quantum dots the magnetic field usually induces at least one singlet-triplet transition,[3,4,7,12–14] reminiscent of the singlet-triplet oscillations in a single dot,[13] before the exchange energy is eventually reduced to zero.

In the present paper we show that at zero magnetic field the exchange energy can be strongly enhanced by an asymmetry introduced in the confinement potential of laterally coupled dots. At high magnetic fields a small asymmetry[19] turns out to be irrelevant for the exchange energy which vanishes (when the Zeeman spin effect is neglected) due to a complete localization of electrons in different dots.

Asymmetry of the confinement potential in existing devices containing laterally coupled dots[9,10] is the rule. In fact symmetric coupling appears only for voltages along the diagonal[20] connecting the triple points at the honeycomb stability diagram.[10] Although vertical coupling of asymmetric dots[4] has been considered in the context of the exchange energy, most[3,12,13] of the theoretical work on laterally coupled dots dealt with pairs of identical dots. Only recently was the effect of the asymmetry on the few-electron charging considered.[9] The influence of asymmetry on the exchange energy in laterally coupled dots was addressed in Ref. 3 where the effect of the electric field was studied in the Heitler-London approximation assuming single occupancy of the dots with a neglected dependence of the single-electron wave functions on the magnetic field. This neglect leads[3] to a magnetic-field-independent shift of the exchange energy, which is in disagreement with the exact diagonalization results presented below.

We consider a two-dimensional double quantum dot in a perpendicular magnetic field $\boldsymbol{B}=(0,0,B)$ and neglect the spin Zeeman effect, which does not influence the orbital wave functions, and which can be trivially accounted for as a shift linear in B to the exchange energy.[21] The Hamiltonian of the pair reads

$$H = H_1^s + H_2^s + e^2/4\pi\epsilon\epsilon_0 r_{12}, \tag{1}$$

where ϵ is the dielectric constant and H^s the single-electron Hamiltonian

$$H^s = (-i\hbar\nabla + e\boldsymbol{A})^2/2m^* + V(x,y), \tag{2}$$

with m^* the electron band mass and $V(x,y)$ the potential of two Gaussian[22,23] dots

$$V(x,y) = -V_l e^{-[(x+d/2)^2+y^2]/R^2} - V_r e^{-[(x-d/2)^2+y^2]/R^2}, \tag{3}$$

where V_l and V_r are the depths of the left and right dots, respectively, d is the distance between the dot centers, and R is the radius of each of the dots. It was recently found[24] that the confinement energy as generated electrostatically in a gated two-dimensional electron gas is largest when the po-

tential has a Gaussian shape. The single-electron eigenfunctions of Hamiltonian (2) are obtained in the Landau gauge $\boldsymbol{A}=(-By,0,0)$ using a basis $\Psi_\mu(\boldsymbol{r})=\Sigma_{i=1}^{M}c_i^\mu\psi_{\boldsymbol{R}_i}(\boldsymbol{r})$ of the lowest Landau level eigenfunctions centered around points $\boldsymbol{R}_i=(X_i,Y_i)$:[18,25–27]

$$\psi_{\boldsymbol{R}_i}(\boldsymbol{r}) = \sqrt{\alpha_i}\exp\{-\alpha_i(\boldsymbol{r}-\boldsymbol{R}_i)^2/4 + ieB(x-X_i)(y+Y_i)/2\hbar\}/\sqrt{2\pi}. \quad (4)$$

Two-electron eigenfunctions $\chi(\boldsymbol{r}_1,\boldsymbol{r}_2)$ of Hamiltonian (1) are subsequently calculated in a basis of symmetrized (antisymmetrized) products of single-electron wave functions $\Psi_\mu(\boldsymbol{r}_1)\Psi_\nu(\boldsymbol{r}_2)$ for the singlet (triplet) two-electron states. Extensive discussion of the exact diagonalization with wave functions (4) is given in Ref. 18. Here we just remind the reader that the displaced lowest Landau wave functions also reproduce higher Fock-Darwin[1] states. We use 14 centers $\boldsymbol{R}_i$, i.e., 7 centers per dot, one in the center of each dot and six on a circle surrounding it. Radii of both circles as well as parameters α_i responsible for the localization of the wave functions (4) are optimized variationally.[28] Comparing the results for the magnetic field dependence of the exchange energy presented in Fig. 4 of Ref. 13 with the results of the present method applied to the model potential used therein[13] we find a nearly exact agreement with differences that do not exceed 5 μeV. However, contrary to the present approach, the basis used in Ref. 13, consisting of wave functions localized around the origin, is bound to be slowly convergent for larger interdot distances and/or high magnetic fields.

We use the material data of GaAs, $\epsilon=12.9$, $m^*=0.067$, and take the potential parameters $R=30$ nm, $V_r=25$ meV, $d=52$ nm (unless stated otherwise), and the value of V_l is varied to induce the asymmetry. For a single quantum dot ($V_l=0$) the energy spacing between the ground and first excited single-electron energy levels is 6.6 meV and between the first and the second excited energy levels the spacing equals 5.2 meV.

For the explanation of the results presented below we find it useful to introduce the single-electron basis consisting of lowest-energy states s_l, s_r, p_l, p_r, where $s(p)$ stands for the $0(-\hbar)$ angular momentum states and the subscript $l(r)$ denote the localization of the state in the left (right) dot. Figure 1 shows the confinement potential for a symmetric ($V_l=25$ meV) pair of coupled dots and for a pair with a small[19] asymmetry ($V_l=32$ meV). For $B=0$ the asymmetry-induced shift of the charge density to the left (deeper) dot is visibly stronger for the singlet state [see Figs. 1(a) and 1(b)]. At $B=0$ the exchange energy for the asymmetric system of coupled dots presented in Fig. 1(b) equals 0.32 meV and is three times larger than in the symmetric case of Fig. 1(a) for which $\Delta E=0.1$ meV (see below).

At high B the singlet and the triplet charge densities become identical [Figs. 1(c) and 1(d)] for both the symmetric and asymmetric coupling. At high magnetic field for which the probability of double occupancy of each of the dots vanishes (see below) both lowest-energy singlet and the lowest-energy triplet wave functions can be described using the

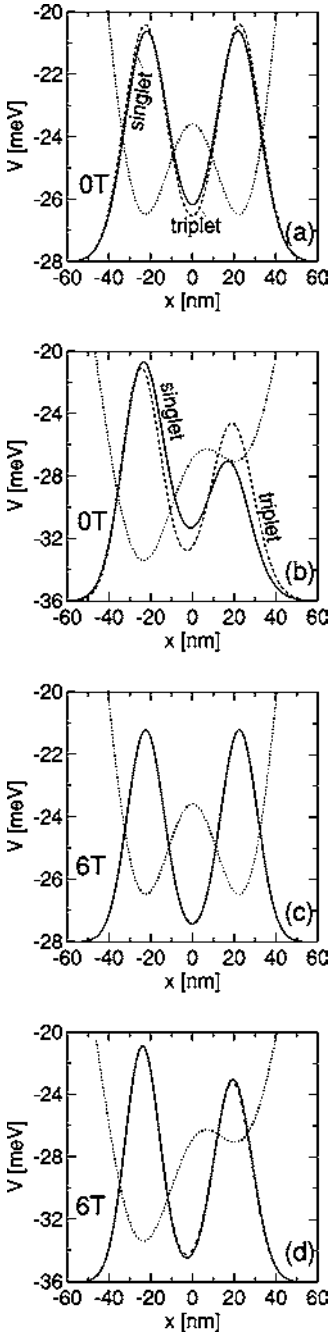

FIG. 1. Confinement potential (dotted line) and singlet (solid line) and triplet (dashed line) charge density plotted in arbitrary units at $y=0$ axis for $V_r=25$ meV and (a) $V_l=25$ meV and $B=0$, (b) $V_l=32$ meV and $B=0$, (c) $V_l=25$ meV and $B=10$ T, (d) $V_l=32$ meV and $B=6$ T.

lowest-energy wave functions localized in the left and right dot

$$\chi(\boldsymbol{r}_1,\boldsymbol{r}_2) = s_l(\boldsymbol{r}_1)s_r(\boldsymbol{r}_2) \pm s_r(\boldsymbol{r}_1)s_l(\boldsymbol{r}_2), \quad (5)$$

with a + sign for the singlet state and − for the triplet state (this function is not normalized). The charge density is obtained by integrating the two-electron probability density over coordinates of one of the electrons

$$\rho(\boldsymbol{r}) = \int d\boldsymbol{r}_2 |\chi(\boldsymbol{r},\boldsymbol{r}_2)|^2$$

$$= |s_l(\boldsymbol{r})|^2 + |s_r(\boldsymbol{r})|^2 \pm 2\mathrm{Re}[s_r^*(\boldsymbol{r}) s_l(\boldsymbol{r}) \int d\boldsymbol{r}_2 s_l^*(\boldsymbol{r}_2) s_r(\boldsymbol{r}_2)]. \quad (6)$$

As the magnetic field increases s_l and s_r wave functions become more strongly localized.[18] Finally, the overlap integral between these functions appearing in Eq. (6) vanishes leading to identical charge densities for the singlet and triplet states (see Fig. 1) and to the singlet-triplet degeneracy (see below). Similarly the singlet and triplet charge densities become indistinguishable in large quantum dots without the external magnetic field.[17] Note that the external magnetic field reduces the effect of the asymmetry on the charge densities [see Figs. 1(b) and 1(d)] due to an increased depth of the effective potential well at the electron localization positions.

Figure 2(a) shows the charge accumulated at the left of the origin $2\int_{-\infty}^{0} dx_1 \int_{-\infty}^{\infty} dy_1 \int d\boldsymbol{r}_2 |\chi(\boldsymbol{r}_1,\boldsymbol{r}_2)|^2$ as a function of the depth of the left quantum dot for $B=0$. For the symmetric system ($V_l=25$ meV) the charge is equally distributed between the dots. For $d=52$ nm near the symmetric point the charge in the left dot for both the triplet and the singlet is approximately a linear function of V_l, but the slope of the straight line for the singlet is more than twice steeper indicating that the triplet state is more robust against the inbalance (V_l/V_r). For larger barrier thickness ($d=60$ nm) the curves acquire a more stepwise character.

The probability of finding both electrons at the same side of the origin $(\int_{-\infty}^{0} dx_1 dx_2 \int_{-\infty}^{\infty} dy_1 dy_2 |\chi(\boldsymbol{r}_1,\boldsymbol{r}_2)|^2 + \int_{0}^{\infty} dx_1 dx_2 \int_{-\infty}^{\infty} dy_1 dy_2 |\chi(\boldsymbol{r}_1,\boldsymbol{r}_2)|^2)$, quantifying the double occupancy of the dots, is plotted as function of V_l in Fig. 2(b) for $d=52$ nm and $B=0$. For the symmetric system the double occupancy probability in the singlet state is almost twice as large as the one in the triplet state. When the left dot is 1/3rd deeper or shallower than the right dot the probability that the deepest dot is double occupied is roughly 50% in the singlet but only 10% in the triplet state.

The dependence of the exchange energy on the asymmetry for $B=0$ is presented in Fig. 2(c). The exchange energy is minimal for the symmetric system (i.e., $V_r=V_l=25$ meV). For a thick interdot barrier ($d=60$ nm) between symmetric dots the exchange energy is 0 due to the negligibly small tunnel coupling and complete charge separation. The exchange energy becomes nonzero only when the charge of both electrons in the singlet state starts to occupy the deepest dot [see Fig. 2(a)]. For thinner barriers [see plots for $d=52$ and 48 nm in Fig. 2(c)] even a small asymmetry increases the exchange energy.

The results of Figs. 2(a)–2(c) can be explained in the following way. In symmetric systems and in systems with a small[19] asymmetry the two-electron singlet (triplet) states consist mainly of the symmetrized (antisymmetrized) products given in Eq. (5). In the singlet state the double occupancy is introduced mainly by symmetric combinations $s_l(\boldsymbol{r}_1)s_l(\boldsymbol{r}_2)$ and $s_r(\boldsymbol{r}_1)s_r(\boldsymbol{r}_2)$, which, however, do not contribute to the triplet state due to the Pauli exclusion. The double occupancy in the triplet state can be realized by admixtures of states $\phi_r = \boldsymbol{A}\{s_r(\boldsymbol{r}_1)p_r(\boldsymbol{r}_2)\}$ and $\phi_l = \boldsymbol{A}\{s_l(\boldsymbol{r}_1)p_l(\boldsymbol{r}_2)\}$ ($\boldsymbol{A}$ stands for the antisymmetrizer). Triplets ϕ_r and ϕ_l correspond to maximum density droplets[1] confined in the right and left dots, respectively. In absence of the magnetic field these states have larger energies than $s_l(\boldsymbol{r}_1)s_l(\boldsymbol{r}_2)$ and $s_r(\boldsymbol{r}_1)s_r(\boldsymbol{r}_2)$ combinations resulting in a smaller double occupancy probability for the triplet state. In the presence of the asymmetry the singlet combination with a doubly occupied s energy level of the deepest dot has the lowest single-electron energy, which increases the double occupancy probability in the singlet state. The probability of the double occupancy in the triplet state also increases with asymmetry [see Fig. 2(b)],

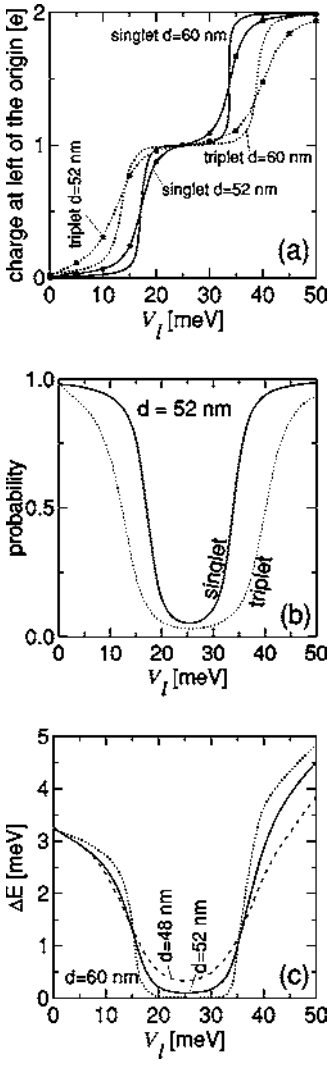

FIG. 2. (a) Charge accumulated at left of the origin for $d=52$ nm and $d=60$ nm in the singlet (solid lines) and triplet (dotted lines) states as function of the depth of the left quantum well V_l. Data for $d=52$ nm are marked with squares. (b) Probabilities that both electrons are on the same side of the origin for the singlet (solid lines) and triplet (dotted lines) states for $d=52$ nm. (c) Singlet-triplet energy difference as function of V_l. The values for $d=48$, 52 and 60 nm are plotted with dashed, solid and dotted lines, respectively.

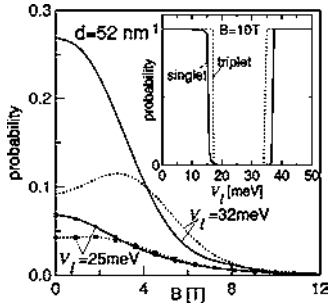

FIG. 3. Probability that both electrons are on the same side of the origin for singlets (solid lines) and triplets (dashed lines) for symmetric (V_l=25 meV) and asymmetric (V_l=32 meV) quantum dots as function of the magnetic field. Curves for the symmetric case are marked by squares. Inset: Same but for B=10 T as function of V_l.

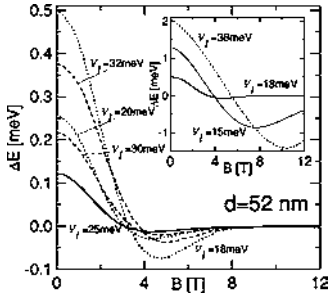

FIG. 4. Exchange energy as function of the magnetic field for V_r=25 meV and various values of V_l for which the electrons at high B occupy different dots. Inset: Exchange energy for V_l=18 meV (same as in the main figure) and for V_l=15 and 38 meV. For the two latter values the deeper dot is doubly occupied at high B.

but more slowly, since in the triplet state the p-excited state of the deepest dot has to be occupied. Therefore, the asymmetry lowers the energy of the singlet with respect to the triplet which explains the exchange energy enhancement by the asymmetry observed in Fig. 2(c).

Figure 3 shows that the double occupancy probability changes as a function of the magnetic field for a symmetric double dot and a double dot with a small[19] asymmetry. In both the symmetric and asymmetric dots the probability for the singlet decreases monotonically to zero with increasing field. A similar high-B limit behavior is observed for the triplet state. However, surprisingly, as the magnetic field is switched on the probability for the triplet initially increases. This is because in the subspace of states with both electrons in the deepest dot the lowest-energy-state undergoes singlet-triplet oscillations[1] as in the single-dot problem. Above a critical value of the magnetic field[29] the maximum density droplet states ϕ_r and ϕ_l acquire lower energy than the singlets built of products of s single-electron states confined in the same dot. This explains why beyond a certain value of the external field the probability of finding both electrons in the same dot is larger in the triplet than in the singlet state.

The discussed singlet-triplet energy crossings for the states confined in the single dot has a striking effect on the capacity of the deepest dot to bind both electrons for larger[19] asymmetry. The inset of Fig. 3 shows the probability that both electrons are in the same dot for B=10 T. Usually in the triplet state the electrons avoid each another more efficiently than in the singlet state due to the Pauli exclusion principle. However, contrary to the case of B=0 [see Fig. 2(b)] for B =10 T (see the inset of Fig. 3) counterintuitively, the electrons in the triplet state occupy the same dot more easily (for smaller asymmetry) than in the singlet state. At high magnetic field the lowest singlet and triplet energy levels corresponding to electrons occupying separate dots are degenerate [see the discussion after Eqs. (5) and (6)] but the lowest-energy state with both electrons in the deepest dot is the triplet maximum density droplet. As a consequence, the lowest triplet becomes localized in the deepest dot for smaller asymmetry than the lowest singlet.

The magnetic-field dependence of the exchange energy is displayed in Fig. 4. The magnetic field inducing singlet-triplet transition increases with the asymmetry, which is more effective for $V_l > V_r$ because of the increased strength of the confinement in the left (deeper) dot which weakens the relative effect of the external field. For large B the exchange energy tends to zero as long as the carriers are localized in separate dots at the high-magnetic field limit (see inset to Fig. 3). This is not the case for strongly asymmetric potentials for which both electrons stay in the same dot and for which the singlet-triplet oscillations continue to higher magnetic fields (see plots for V_l=15 meV and V_l=38 meV in the inset of Fig. 4).

In summary, we have studied the effect of the asymmetry on the lateral coupling of quantum dots in a perpendicular magnetic field using a numerically exact method. We have shown that at B=0 the exchange energy is minimal for a symmetric system of laterally coupled dots, and that the asymmetry promoting double occupancy of the deepest dot in the singlet state can enhance this by a factor of 4. If for practical reasons a stronger coupling between the dots was needed and the dots could not be made any smaller the solution is to make one of them even larger. We showed that for high magnetic fields localization of both electrons in the deepest potential minimum is easier if the electrons have parallel spins and explained this effect in terms of singlet-triplet oscillations in the lowest-energy state with both electrons in the deepest dot.

This paper was partly supported by the Flemish Science Foundation (FWO-Vl), the Belgian Science Policy, the University of Antwerpen (VIS and GOA), and the Polish Ministry of Scientific Research and Information Technology in the framework of the solicited Grant No. PBZ-MIN-008/P03/2003. B.S. was supported by the Foundation for Polish Science (FNP) and by the EC Marie Curie IEF Project No. MEIF-CT-2004-500157. We are grateful to M. Stopa and J. Adamowski for useful discussions.

[1] S. M. Reimann and M. Manninen, Rev. Mod. Phys. **74**, 1283 (2002).
[2] D. Loss and D. P. DiVincenzo, Phys. Rev. A **57**, 120 (1998).
[3] G. Burkard, D. Loss, and D. P. DiVincenzo, Phys. Rev. B **59**, 2070 (1999).
[4] G. Burkard, G. Seelig, and D. Loss, Phys. Rev. B **62**, 2581 (2000).
[5] M. Pi, A. Emperador, M. Barranco, F. Garcias, K. Muraki, S. Tarucha, and D. G. Austing, Phys. Rev. Lett. **87**, 066801 (2001).
[6] M. Bayer, P. Hawrylak, K. Hinzer, S. Fafard, M. Korkusinski, Z. Wasilewski, O. Stern, and A. Forchel, Science **291**, 451 (2001).
[7] D. Bellucci, M. Rontani, F. Troiani, G. Goldoni, and E. Molinari, Phys. Rev. B **69**, 201308(R) (2004).
[8] S. Bednarek, T. Chwiej, J. Adamowski, and B. Szafran, Phys. Rev. B **67**, 205316 (2003).
[9] R. Ravishankar, P. Matagne, J. P. Leburton, R. M. Martin, and S. Tarucha, Phys. Rev. B **69**, 035326 (2004).
[10] W. G. van der Wiel, S. De Franceschi, J. M. Elzerman, T. Fujisawa, S. Tarucha, and L. P. Kouwenhoven, Rev. Mod. Phys. **75**, 1 (2003).
[11] T. H. Oosterkamp, S. F. Godijn, M. J. Uilenreef, Y. V. Nazarov, N. C. van der Vaart, and L. P. Kouwenhoven, Phys. Rev. Lett. **80**, 4951 (1998).
[12] X. Hu and S. Das Sarma, Phys. Rev. A **61**, 062301 (2000).
[13] A. Harju, S. Siljamäki, and R. M. Nieminen, Phys. Rev. Lett. **88**, 226804 (2002).
[14] M. Marlo-Helle, A. Harju, and R. M. Nieminen, Physica E (Amsterdam) (to be published), cond-mat/0408178.
[15] M. Stopa, S. Tarucha, and T. Hatano, Physica E (Amsterdam) (to be published).
[16] J. Kyriakidis, M. Pioro-Ladriere, M. Ciorga, A. S. Sachrajda, and P. Hawrylak, Phys. Rev. B **66**, 035320 (2002).
[17] B. Szafran, F. M. Peeters, S. Bednarek, T. Chwiej, J. Adamowski, and A. Dabrowska, Phys. Rev. B **70**, 035401 (2004).
[18] B. Szafran, F. M. Peeters, S. Bednarek, and J. Adamowski, Phys. Rev. B **69**, 125344 (2004).
[19] We consider the asymmetry to be *small* if at high magnetic field each of the dots is singly occupied in the ground state in contrast to the *large* asymmetry case for which only the deepest dot is occupied.
[20] For two electrons those in which $\mu_{11}=\mu_{10}=\mu_{01}$ and $\mu_{11}=\mu_{21}=\mu_{12}$, where μ_{ij} is the chemical potential of $i+j$ electrons, with i electrons in one dot and j in the other, see Ref. 10.
[21] Zeeman singlet-triplet splitting is $B\hbar g^*\mu_B$, where g^* is the effective Landé factor and μ_B the Bohr magneton. For GaAs this splitting is $0.025B$ meV/T.
[22] J. Adamowski, M. Sobkowicz, B. Szafran, and S. Bednarek, Phys. Rev. B **62**, 4234 (2000).
[23] J. Kolehmainen, S. M. Reimann, M. Koskinen, and M. Manninen, Eur. Phys. J. B **13**, 731 (2000).
[24] S. Bednarek, B. Szafran, K. Lis, and J. Adamowski, Phys. Rev. B **68**, 155333 (2003).
[25] C. Yannouleas and U. Landman, Phys. Rev. B **66**, 115315 (2002).
[26] J. Kainz, S. A. Mikhailov, A. Wensauer, and U. Rössler, Phys. Rev. B **65**, 115305 (2002).
[27] B. Szafran and F. M. Peeters, Europhys. Lett. **66**, 701 (2004).
[28] We use two different variational parameters α_r and α_l for the seven centers associated with the right and the left dot, respectively.
[29] In a *single* dot the first spin-polarized ground-state appears between $B=5$ T and 15 T for $V=25$ meV and between $B=6.5$ T and 19.5 T for $V=35$ meV.

Three electrons in laterally coupled quantum dots: Tunnel vs electrostatic coupling, ground-state symmetry, and interdot correlations

B. Szafran[1,2] and F. M. Peeters[1]
[1]*Departement Fysica, Universiteit Antwerpen (Campus Drie Eiken), B-2610 Antwerpen, Belgium*
[2]*Faculty of Physics and Applied Computer Science, AGH University of Science and Technology, al. Mickiewicza 30, 30-059 Kraków, Poland*
(Received 16 November 2004; published 21 June 2005)

The phase diagram for the ground-state symmetry of three electrons confined in a pair of laterally coupled dots is determined as function of the interdot distance and the magnetic field. With a few exceptions the ground-state spin and parity symmetry sequence of a circular harmonic quantum dot is conserved. Reentrant behavior of some energy levels as ground states is found as a function of the magnetic field. The disappearance of interdot tunnelling due to a strong magnetic field leads to ground-state degeneracy of the even and odd parity energy levels. It is shown that at a high magnetic field the system can be closely approximated by a two-electron system confined in one dot and a spectator electron localized in the other. Broken-parity eigenstates with a classical charge distribution are constructed and used to discuss the interdot electron-electron correlations.

DOI: 10.1103/PhysRevB.71.245314 PACS number(s): 73.21.La

I. INTRODUCTION

Electrons confined in coupled quantum dots[1–25] form systems commonly referred to as artificial molecules with single-electron wave functions forming bonding and antibonding orbitals similar to those known from the quantum chemistry of covalent molecules. Artificial molecules are formed by vertically[1–11] coupled dots or by dots coupled laterally.[12–25] The electronic properties of two-electron systems in vertically[4–7] as well as laterally[12–16] coupled dots have been extensively studied by exact methods that for two electrons are particularly convenient due to the separation of the spatial and spin degrees of freedom. The two-electron studies were mainly motivated by the proposed[26] realization of a quantum gate based on the spins of the electrons confined in coupled dots. For larger electron numbers the mean field methods[1–3,18–21] are more commonly used. The mean field approaches give reliable estimates for the ground-state energy and are useful in simulations[2,3,18,19,27] of devices but they possess several shortcomings[28] due to an approximate treatment of the electron-electron correlations, which results in artifactal symmetry-breaking effects leading to an oversimplified picture of Wigner crystallization, to the appearance of spin-density waves, etc.

The exact solution of the few-electron Schrödinger equation possesses a rich literature for circular two-dimensional quantum dots.[28–39] Less work has been done in noncircular[40–42] and vertically coupled quantum dots.[8–11] In this paper we present the exact diagonalization results for the three-electron system in quantum dots coupled laterally. We are unaware of any previous exact diagonalization calculations for a pair of laterally coupled dots with more than two electrons. While in vertically coupled dots the interdot tunnelling makes the problem intrinsically three dimensional, but with conserved axial symmetry, in the laterally coupled dots the physical interest (and technical implementation difficulties) are related to the two-center nature of the electron localization.

The three-electron system in laterally coupled dots is more interesting than the extensively discussed two-electron problem[12–16] for at least two reasons: (1) In the two-electron system the electron charge localized in each of the identical dots is exactly equal to e.[16] On the other hand, the three-electron system possesses two equivalent classical configurations with two electrons in the left or right dot. We show that the three-electron parity operator eigenstates can be constructed as superpositions of the states corresponding to both classical configurations. The charge density distribution in the parity eigenstates is nonclassical; with one and one-half electron charge confined in each of the dots. Due to tunnelling each attempt to localize two electrons in one of the dots will result in the formation of a nonstationary state. The classical charge distribution can only be obtained when the tunnel coupling between the dots disappears. The previous mean field analysis of the charge distribution and symmetries dealt mostly with an even number of electrons[20–22] for which the problem of nonclassical charge distribution, likely to result in an artifactal spatial symmetry breaking, is absent. (2) The evolution of the two-electron ground state ends in the singlet-triplet degeneracy[12–16] when the tunnel coupling is removed by an external magnetic field. On the other hand, in the three-electron system at high-magnetic field, spin oscillations should be expected to continue in the two-electron subsystem perturbed by the Coulomb potential of the electron confined in the other dot and the electrostatic interdot coupling should pin[43–45] the magnetic-field induced two-electron Wigner molecules, extracting them from the internal coordinates of the two-electron system to the laboratory frame of reference.

In this paper we study the spin and parity symmetry of the three-electron ground state, the electron-electron correlation, the Wigner crystallization, and the extinction of tunnel coupling in the limit of high magnetic field. The high-magnetic field spectra are explained using a single-dot two-electron model, including the Coulomb potential of an electron local-

ized in the other dot. The interdot electron-electron correlations accompanying the electrostatic interdot coupling, are studied using broken-parity eigenstates. The results presented in this paper have been obtained by the multicenter configuration interaction method described in detail in Ref. 41. This method was previously applied to problems of Wigner crystallization in low-symmetry quantum dots,[41] to pinning of Wigner molecules by an external Coulomb defect,[45] and to the effect of the asymmetry on the exchange energy in two-electron laterally coupled dots.[16]

The present paper is organized as follows. In Sec. II we present the theory, Sec. III contains the results, summary and conclusions are given in Sec. IV.

II. THEORY

We consider three electrons bound in a two-dimensional system of laterally coupled dots that is described by the Hamiltonian,

$$H=\sum_{i=1}^{3} h_i+\sum_{i=1}^{3}\sum_{j>i}^{3}\frac{e^2}{4\pi\epsilon\epsilon_0 r_{ij}}, \tag{1}$$

with the single-electron energy operator h defined as

$$h=\frac{1}{2m^*}(-i\hbar\,\boldsymbol{\nabla}+e\mathbf{A})^2+V(x,y), \tag{2}$$

where m^* is the electron effective band mass and ϵ is the dielectric constant. We apply the model potential for laterally coupled dots used previously by several authors,[14,15,20,22]

$$V(x,y)=\frac{m^*\omega_0^2}{2}(\min\{(x-d/2)^2,(x+d/2)^2\}+y^2), \tag{3}$$

where $\hbar\omega_0$ is the confinement energy and d is the distance between the centers of the two dots. For $d=0$ this model potential reduces to a single circular quantum dot with a harmonic oscillator confinement potential.

We use the Landau gauge $\mathbf{A}=(-By,0,0)$, GaAs material parameters[14] $m^*/m_0=0.067$, $\epsilon=12.4$, and choose $\hbar\omega_0=3$ meV for the confinement potential energy. We include only the orbital effects for the ground-state spin and spatial symmetries, but we neglect the spin Zeeman effect. The latter can be trivially taken into account as a shift linear in B to the calculated energy levels. At a high magnetic field the spin Zeeman effect removes the nonpolarized states from the ground-state symmetry sequence, as discussed previously.[28,37,38]

We first solve the single-electron Schrödinger equation in a basis of displaced lowest Landau level eigenfunctions[41,45–48]

$$\Psi_\mu(\mathbf{r})=\sum_{i=1}^{M} c_i^\mu \psi_{\mathbf{R}_i}(\mathbf{r}), \tag{4}$$

where

$$\psi_{\mathbf{R}_i}(\mathbf{r})=\sqrt{\alpha}\exp\{-\alpha(\mathbf{r}-\mathbf{R}_i)^2/4+ieB \times(x-X_i)(y+Y_i)/2\hbar\}/\sqrt{2\pi}, \tag{5}$$

and $\mathbf{R}_i=(X_i,Y_i)$ is the center of localization of the ith basis element. For a single quantum dot the multicenter basis (4) reproduces[41] also the Fock-Darwin eigenfunctions of the higher Fock-Darwin bands that tend to excited Landau levels at a high magnetic field. Therefore, for a single quantum dot the present scheme works as efficient as the ones employing the Fock-Darwin single electron basis.[29–38,48] Since the centers can be chosen quite arbitrarily the multicenter method is suitable to treat any low-symmetry smooth confinement potential.[41] In the present calculations we use 14 centers (7 per dot). The set of centers corresponding to the right quantum dot is chosen in the following way. A single center is localized in the point $(a,0)$. Six additional centers are put around this point on a circle of radius R. The position of the centers for the left dot are obtained from the set associated with the right dot by a change of the sign of the x coordinates. The basis is optimized by taking R, a, and α as variational parameters that are chosen to minimize the energy of the three-electron system.

The three-electron Hamiltonian (1) is diagonalized on the basis of Slater determinants constructed from the single-electron spin orbitals obtained as products of the spatial wave functions expanded in the basis (4) and the eigenfunctions of the z component of the single-electron spin. Eigenstates of Hamiltonian (1) are also eigenstates of the parity operator as well as of the operators of the z component of the total spin (with eigenvalue $S_z\hbar$) and of the square of the total spin $(S(S+1)\hbar^2)$. Of all 3276 three-electron Slater determinants that can be constructed of the 28 spin orbitals we retain only those with the required S_z and parity eigenvalues, which gives a basis of 182 basis elements for $S_z=\pm 3/2$ and 637 basis elements for $S_z=\pm 1/2$. The quantum number of the total spin S is identified for each energy level by its multiplicity ($2S+1$—the degeneracy of the given energy level with respect to S_z). In the following the even (odd) symmetry states are denoted by ^{S}E (^{S}O).

III. RESULTS

A. Energy spectra

Figures 1(a) and 1(b) show the low-energy spectrum of the three-electron single quantum dot ($d=0$). We display energies calculated with respect to the lowest Fock-Darwin energy level, i.e., we subtract $3E_D=3\times\hbar\sqrt{\omega_0^2+\omega_c^2/4}$ from the eigenvalues of Hamiltonian (1). In the absence of the magnetic field the ground state corresponds to -1 angular momentum (in $\hbar$ units). The ground-state angular momentum takes subsequent negative integer values (the absolute value of the angular momentum of the states is given in the figure) as the magnetic field increases. Ground states with angular momentum quantum numbers being multiples of 3 are realized by the spin-polarized states.[28,34,37,49] At lower magnetic field the intervals corresponding to subsequent ground state symmetries have distinctly different lengths [see Fig. 1(a)]. In particular, a larger stability of the ground state with odd angular momentum quantum numbers up to -7 is observed. The results of Fig. 1(a) are in perfect agreement with the results of Mikhailov and Savostianova[37] (cf. Figs. 1(a) and 2(a) of Ref. 37, $\hbar\omega_0=3$ meV corresponds to the interaction

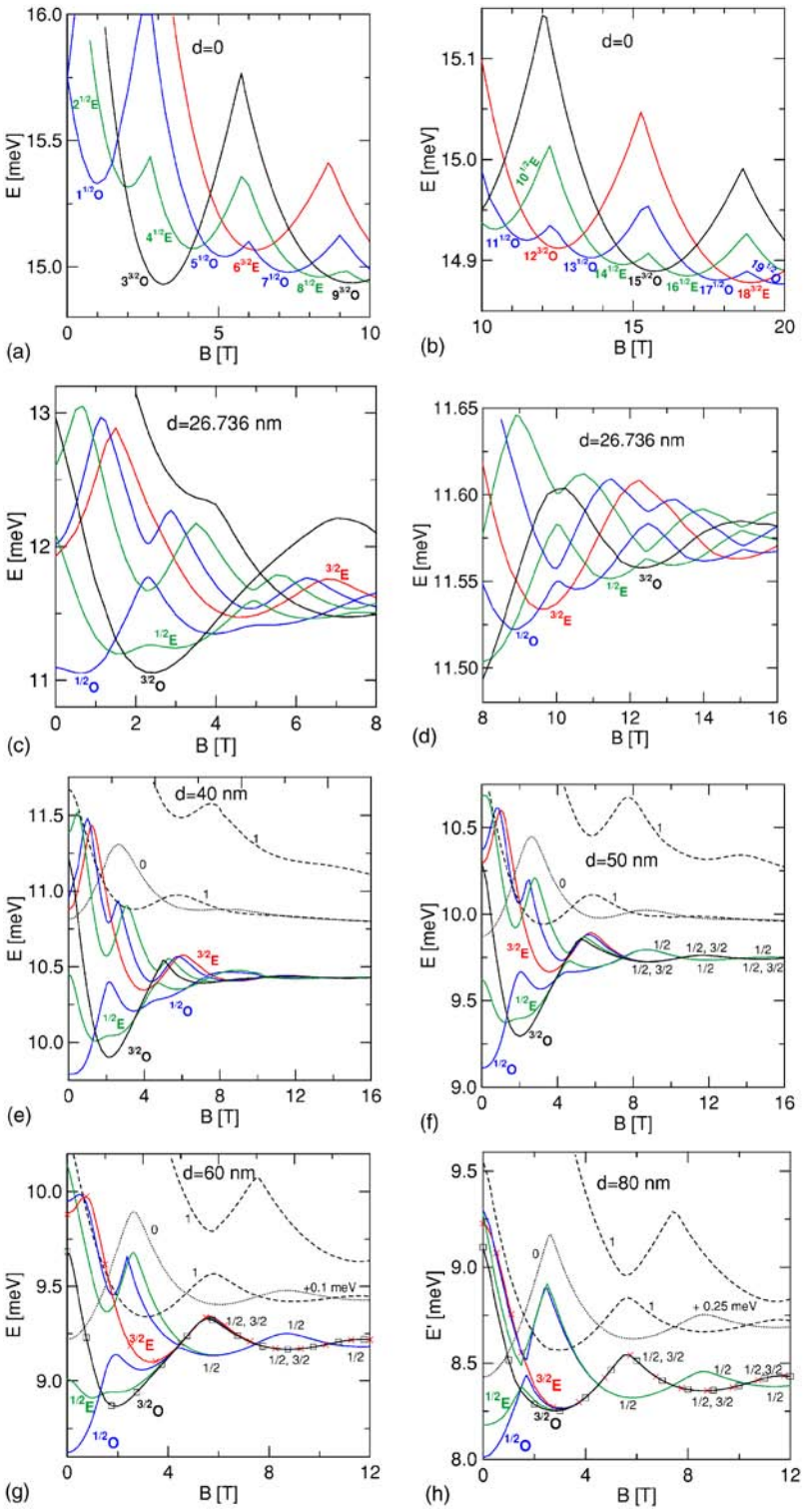

FIG. 1. (Color online) Magnetic field dependence of the three electron spectra for different values of the interdot distance d. Energy levels of $^{1/2}$O, $^{3/2}$O, $^{1/2}$E, and $^{3/2}$E symmetry states are plotted in blue, black, green, and red, respectively. Numbers in the energy levels labels given in (a) and (b) stand for the absolute value of the angular momentum in $\hbar$ units. Dotted and dashed lines in (e–g) show the singlet and triplet energy levels in a reference two-electron system confined in the potential given by Eq. (6). Crosses and squares in (g) and (h) mark the energy levels of spin-polarized states of even and odd parity, respectively. Numbers 0, 1, 1/2, and 3/2 in Figs. 1(e)–1(h) give the spin quantum number of the plotted energy levels. For clarity, the two-electron spectrum in (g) and (h) was shifted by +0.1 and +0.25 meV, respectively.

parameter $\lambda = 1.988$). At higher fields [cf. Fig. 1(b)] the states with increasing angular momentum become the ground state in intervals of nearly constant length in magnetic field. A similar feature has previously been observed in the spin-polarized three-electron system in the Wigner crystallization regime.[48]

Figures 1(c) and 1(d) present the spectrum for coupled dots with centers separated by a distance of $d = 26.736$ nm. In a single circular dot energy levels of the same spin and parity symmetry differ by their angular momentum and cross. Notice that in the coupled dots these crossings are replaced by anticrossings. Apparent crossings of $^{3/2}$O and $^{1/2}$O energy levels around 5.5 and 7.5 T visible in Fig. 1(c) are in fact anticrossings of width 2 μeV. The spectrum conserves the same sequence of the ground-state spin and parity symmetries of the single dot case [cf. Figs. 1(a) and 1(b)]. The only difference is that the $^{3/2}$E state (the ground state for $d = 0$ around 5.6T) is replaced by the $^{1/2}$O energy level stemming

from the mixture of states which in circular quantum dots possess −5 and −7 angular momenta. The $^{1/2}$O energy level is particularly stable as the ground state [cf. Fig. 1(a)] and exhibits reentrant behavior. At higher magnetic field [see Fig. 1(d)] the ground-state changes almost periodically with B like in the single dot case presented in Fig. 1(b), only the length of the magnetic field corresponding to subsequent states of the sequence becomes shortened from about 1.1 to 0.9 T. At high magnetic field the energy differences between the energy levels of different parity becomes smaller with respect to the single dot case presented in Fig. 1(b). For both $d=0$ and $d=26.736$ nm the energy difference between the lowest even and odd spin-polarized energy levels possesses a local maximum near $B=12$ T. For $d=0$ this difference is around 0.25 meV [cf. Fig. 1(b)] while for $d=26.736$ nm it is only 0.05 meV [cf. Fig. 1(d)].

Figure 1(e) shows the spectrum for $d=40$ nm. For $B<10$ T the ground-state-symmetry sequence of the $d=26.736$ nm case is reproduced. Near 8.5 T both the spin-polarized and spin-nonpolarized energy levels become degenerate. For larger barrier thickness the ground state becomes degenerate with respect to parity around 7, 6 and 4 T, for $d=50$, 60, and 60 nm, respectively, [see Figs. 1(f)–1(h)]. The magnetic field leads to an increase of the electron localization in each of the dots, enhancing the effective barrier height and leading finally to vanishing interdot tunnel coupling. This is at the origin of the even-odd degeneracy, similarly as in the single electron problem.

For an interdot separation of $d=40$ nm, the low-energy spectrum collapses into a narrow energy range for large magnetic fields. For $B>12$ T the difference between the lowest energy levels becomes smaller than 0.02 meV [see Fig. 1(e)]. But, for a larger interdot distance we notice, e.g., for $d=50$ nm [cf. Fig. 1(f)] above 8 T distinct spin-related oscillations of the ground-state energy. Up to 10.5 T and between 13.5 and 17 T the two spin-polarized ground states of odd and even symmetry are degenerate with two nonpolarized states of both spatial symmetries. Between 10.5 and 13.5 T the ground state is nonpolarized. The amplitude of these spin oscillations decreases with magnetic field but increases with interdot distance. For instance, the local maximum of the energy splitting between the lowest spin-polarized and nonpolarized energy levels near 12 T is 0.03, 0.04, and 0.06 meV for $d=50$, 60, [see Fig. 1(g)] and 80 nm [see Fig. 1(h)], respectively.

B. Two-electron subsystem and a spectator electron in the other dot

One may expect that in the absence of a tunnel effect, i.e., for larger d and high magnetic field, the system can be reduced to a spectator electron sitting in one dot and two electrons confined in the other dot. In order to verify this hypothesis, we have performed two-electron calculations for a single dot with harmonic oscillator confinement potential perturbed by the Coulomb potential of the electron sitting in the other (left) dot, namely, for the external potential we took

$$V_s(x,y) = \frac{m^*\omega_0^2}{2}(x-d/2)^2 + \frac{e^2}{4\pi\epsilon\epsilon_0}\frac{1}{\sqrt{(x+d/2)^2+y^2}}. \quad (6)$$

Obviously, in the presence of the Coulomb interdot coupling the spectator electron will be shifted off the center of the left quantum dot, but we neglect this shift for simplicity. Two electron calculations were performed with the multicenter configuration interaction method with eight centers put on a circumference of an ellipse and the ninth one in its center. Position of the ellipse center as well as its x and y sizes are optimized variationally. In Figs. 1(e)–1(h) the lowest singlet energy level and the two lowest triplet energy levels are plotted with dotted and dashed lines, respectively. The width of the presented avoided crossings of the spin polarized energy levels can be considered as a measure of the potential deviation from circularity; as discussed in Ref. 45. In the circular quantum dot limit of infinite d, the avoided crossings are replaced by crossings of the magic angular momenta eigenstates corresponding to the semiclassical Wigner distribution of electrons in the inner coordinates. The larger the deviation of the potential from circularity the stronger is the mixing of the states corresponding to neighbor angular momenta from the magic sequence, and, consequently, the wider the anticrossing.[45] The width of the anticrossing appearing near 6 T decreases from 0.7 meV for $d=40$ nm to 0.3 meV for $d=60$ nm and to 0.2 meV for $d=80$ nm. A comparison of Figs. 1(e)–1(h) shows that the singlet-triplet oscillations in the two-electron system have the smallest amplitude for the smallest d for which the perturbation of the harmonic potential is the largest. This finding is consistent with the recent study[52] of the magnetic field effect on the two-electron anisotropic quantum dots showing that the amplitude of the singlet-triplet oscillations[53] disappears with increasing degree of asymmetry and is finally replaced by the singlet-triplet degeneracy in the quasi one-dimensional limit [50,51] of the extreme anisotropy. In circular quantum dots the states of higher angular momentum are less strongly localized. Magnetic field increases the electron localization and consequently the electron-electron interaction in each of the states. This leads to the ground-state angular momentum transitions. For two electrons the ground-state of the center-of-mass corresponds to zero angular momentum so that the entire angular momentum is carried by the relative electron-electron motion. The relative-motion states with odd (even) parity angular momentum quantum numbers are spin triplets (singlets). Therefore, the increase of the angular momentum is accompanied by singlet-triplet oscillations.[53] Magnetic field evolution is different for strongly anisotropic quantum dots in which the two electrons occupy the opposite extremities of the quantum dot potential and the external magnetic field simply increases the localization of each of the electrons leading eventually to the disappearance of the overlap of their wave functions which results in the singlet-triplet degeneracy[54] (vanishing exchange energy). As the interdot distance d increases, the potential becomes more circular which is the reason why the amplitude of the singlet-triplet energy oscillations becomes larger.[52]

The three-electron spectra presented in Figs. 1(e)–1(h) display a striking similarity to the reference two-electron calculations at a high magnetic field. Therefore, at high magnetic field the system is indeed separable into two subsystems confined in different dots. The single electron confined in one of the dots does not participate in the magnetic field evolution of the spectrum and its only role is to perturb the circular symmetry of the confinement potential

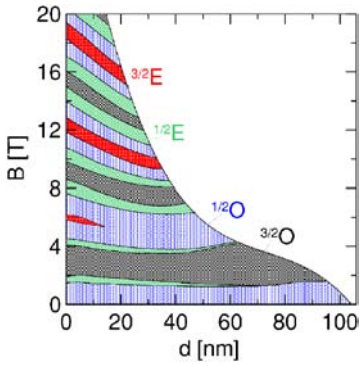

FIG. 2. (Color online) Magnetic field-interdot distance phase diagram for the ground-state symmetry. Blue, green, black, and red regions correspond to a ground state with $^{1/2}$O, $^{1/2}$E, $^{3/2}$O, and $^{3/2}$E symmetry, respectively. The white region corresponds to a negligible interdot tunnel coupling and a near degeneracy of the ground state with respect to spatial parity symmetry.

felt by the two electrons in the other dot. Obviously the three-electron system can be spin polarized only if the two-electron subsystem is spin polarized, which explains the spin dependence of the three-electron low-energy spectrum at a high field [cf. Fig. 1(e)–1(h)]. The discussed spin oscillations in the three-electron system have a somewhat larger amplitude that is due to an exaggerated anisotropy of the external potential in the two-electron reference calculation. The point charge assumed in potential (6) deforms the quantum dot circular potential more strongly than the real charge of the spectator electron, which is in fact diffuse and displaced to the left (see below) from the center of the left dot.

C. Phase diagram for the ground-state symmetry

Our results for the ground-state symmetry and the extinction of the interdot tunnel coupling is summarized in a *d*-*B* phase diagram presented in Fig. 2. The $^{3/2}$E ground state around 6 T disappears for $d>14$ nm. Similarly, the ground state of $^{1/2}$E symmetry around 2 T located between the $^{1/2}$O and $^{3/2}$O ground states disappears above $d>70$ nm. The border of the white region of the phase diagram corresponds to negligible tunnel interdot coupling and was determined as the line beyond which the energy difference between the ground state and the lowest excited state of the same spin but opposite spatial parity is smaller than 0.02 meV.

D. Charge density evolution

The evolution of the ground-state charge density as a function of the external magnetic field is presented in Fig. 3 for $d=26.736$ nm. The charge density exhibits two maxima near $x=\pm 28$ nm. In each of the subsequent ground states, localization of electrons in the left and right dots becomes stronger. For low magnetic fields the shape of the charge density is similar to the one of the three-electron ellipsoidal quantum dot (cf. Fig. 4 in Ref. 41). Nevertheless, at higher magnetic field the three-electron charge density in the ellipsoidal dot develops two maxima along the *y* axis[41] related to the position of one of the electrons in the two classically degenerate configurations. Figure 3 shows a different behavior: the electron charge density is removed from the *y* axis at which the barrier potential energy is maximal. Note that in the state $^{3/2}$E at 5 T [cf. Fig. 3(l)] the central hole in the charge density is larger than in the ground states for the neighboring range of magnetic fields [cf. Figs. 3(e)–3(h)].

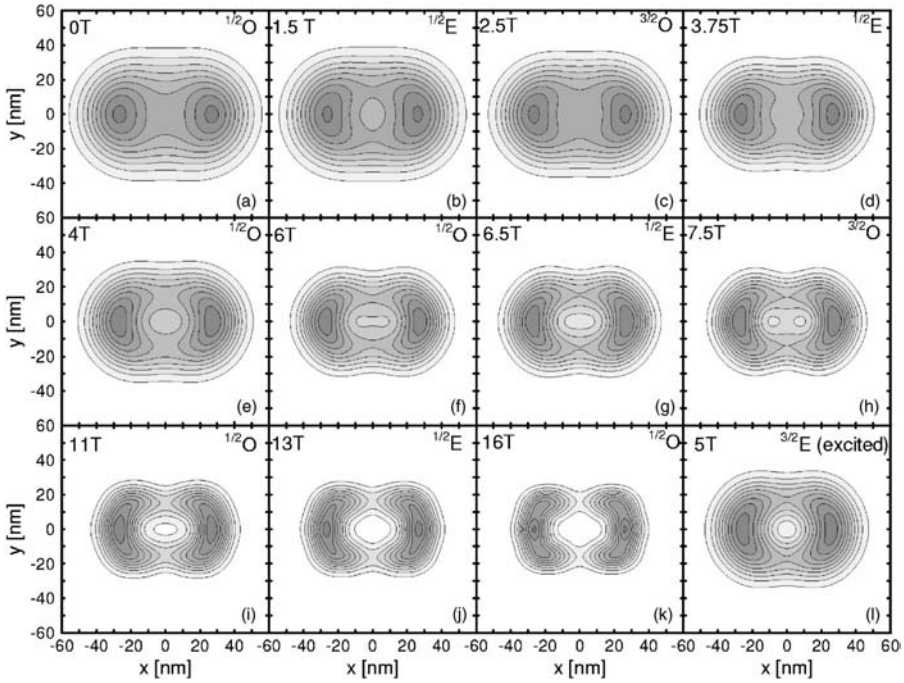

FIG. 3. Contour plots of the charge density for $d=26.736$ nm and various magnetic fields. The plots (a–k) correspond to the ground state. Plot (l) at $B=5$ T corresponds to an excited state of $^{3/2}$E symmetry.

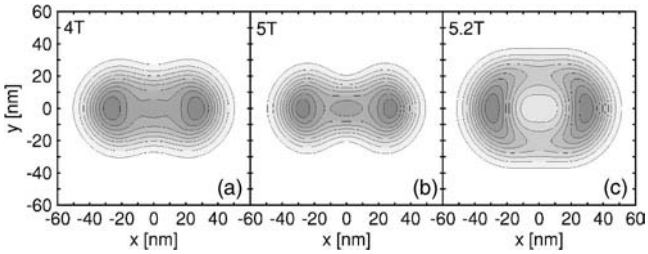

FIG. 4. Charge density contours for the lowest-energy state of $^{3/2}$O symmetry for various values of the magnetic field and $d=26.736$ nm.

This is the reason why this symmetry is replaced by the $^{1/2}$O symmetry [cf. Figs. 1(c) and 2] in the ground state.

Increasing the magnetic field leads to an increased electron localization in each of the states. For a given magnetic field the subsequent states in the ground-state symmetry sequence correspond to weaker electron localization. In order to keep the interelectron distances approximately constant as the magnetic field increases, the system has to change the symmetry of the ground state. The mechanism for ground-state symmetry transformations is therefore the same as the one in circular quantum dots (see Sec. III B). Between the avoided level crossings, the increased localization in each of the states induced by increasing the magnetic field is usually not accompanied by any pronounced quantitative change of the shape of the charge density droplet. An exception to this rule is observed for the $^{3/2}$O state. Figure 4 shows the charge density of this state for magnetic field values for which this state is no longer the ground state. For 4 T a "bridge" of an increased density along the x axis appears [compare Fig. 3(c) and Fig. 4(a)]. Just before the narrow avoided crossing near 5.1 T [cf. Fig. 1(d)], a third charge density maximum is formed in the barrier around the origin [see Fig. 4(b)]. In this way the system forms a quasi-one-dimensional Wigner molecule[50,51,54] with all charge maxima situated along the x axis. Recently, it was proven[54] that the spatial parity of the spin polarized three-electron state must be odd in order to allow the state to form such a one-dimensional Wigner molecule. After the anticrossing of spin polarized odd parity energy levels near 5.1 T, the lowest state of this symmetry possesses a central charge density hole [cf. Fig. 4(c)]. The shape of the charge density of this state, when it becomes the ground state, is displayed in Fig. 3(h).

Let us now look at the magnetic-field dependence of the electron-electron correlations. Figure 5 shows the contour plots for the pair correlation function[39] when the position of one of the electrons is fixed at the point $(-28\ \text{nm}, 0)$. For $B<6$ T the two other electrons are simply shifted to the right-hand side of the double quantum dot potential. Only for $B>6$ T the two distinct centers of electron localization in the right quantum dot appear. Wigner localization around these centers, which coincide with the position of classical electrons[55] in the lowest-energy configuration,[41] becomes more pronounced at higher magnetic fields. Fig. 5(l) shows the excited $^{3/2}$E energy level. Besides a larger central charge density hole [see Fig. 3(l)] this state exhibits also a stronger electron-electron correlation than the ground state [cf. Figs. 5(e) and 5(f)] in this magnetic field range.

E. Broken-parity solutions and interdot correlations

For the parity operator eigenstates discussed so far one cannot tell in which of the dots the two electrons are localized. Let us now consider construction[41] of the stationary states with a classical charge density distribution with two electrons confined in a specified left or right dot.

In single quantum dots the classical degeneracy,[41] i.e., the existence of more than one classical lowest-energy configuration of electrons, is accompanied by crossings of levels of different symmetries. Superpositions of the two states corresponding to the crossing levels allows us to extract[41] one of the classical configurations. Here we use a similar manipulation, constructing a superposition of odd (O) and even (E) parity wave functions,

$$X = (E + \exp(i\phi)O)/\sqrt{2}. \tag{7}$$

The state described by the wave function X is not an eigenstate of the parity operator but at the even-odd degeneracy points appearing at the level crossings, or for negligible tunnel coupling, it is still stationary, i.e., it is still the energy eigenstate.

For $d=26.736$ nm near $B=8.75$ T, level crossings of odd and even parity energy levels appear [cf. Fig. 1(d)] for both $S=1/2$ and $S=3/2$ states. We use this degeneracy to illustrate the properties of the broken-parity Hamiltonian eigenstates. Figure 6 shows the charge accumulated on the right-hand side of the $y=0$ axis as a function of the phase ϕ in Eq. (7). Notice that in the singlet broken-parity state the right dot can contain up to 1.64 of the elementary charge. For the triplet the maximum value is $1.89e$. The maximum value of the charge localized in the right dot reaches $2e$ (see the curve for $d=80$ nm) only when the tunnel coupling is completely removed by the application of a high magnetic field and/or for a large barrier thickness.

The charge density of the degenerate-energy spin-polarized states at $B=8.75$ T is displayed in Fig. 7(a) (the even parity state) and Fig. 7(b) (the odd parity state). Figure 7(c) shows the broken-parity state constructed of the two spin-polarized parity eigenstates for the phase in Eq. (7) for which the charge localized at the $x>0$ semiplane is maximal [cf. Fig. 6]. Figure 7(c) shows that in spite of the leakage of the two-electron charge through the barrier to the region of negative x, the charge of the third electron is distinctly separated. Such a separation is not visible in the singlet state plotted in Fig. 7(d). According to Eq. (7) both odd and even parity states can be reconstructed from two broken-parity states with two electrons localized in the right and left dot. This is visible in the pair-correlation function plots presented in Figs. 7(e) and 7(f) for the odd-parity spin-polarized state. Depending on the choice of the fixed-electron position a configuration with two electrons in the left [cf. Fig. 7(e)] or right dot [cf. Fig. 7(f)] appears in the pair-correlation function plots. This property of the parity eigenstates makes it difficult to visualize the interdot correlations between the electron positions: instead of the reaction of the charge localized in one dot to the position of an electron in the other, switching between configurations is observed. However, the effect of interdot correlations can be conveniently visualized using

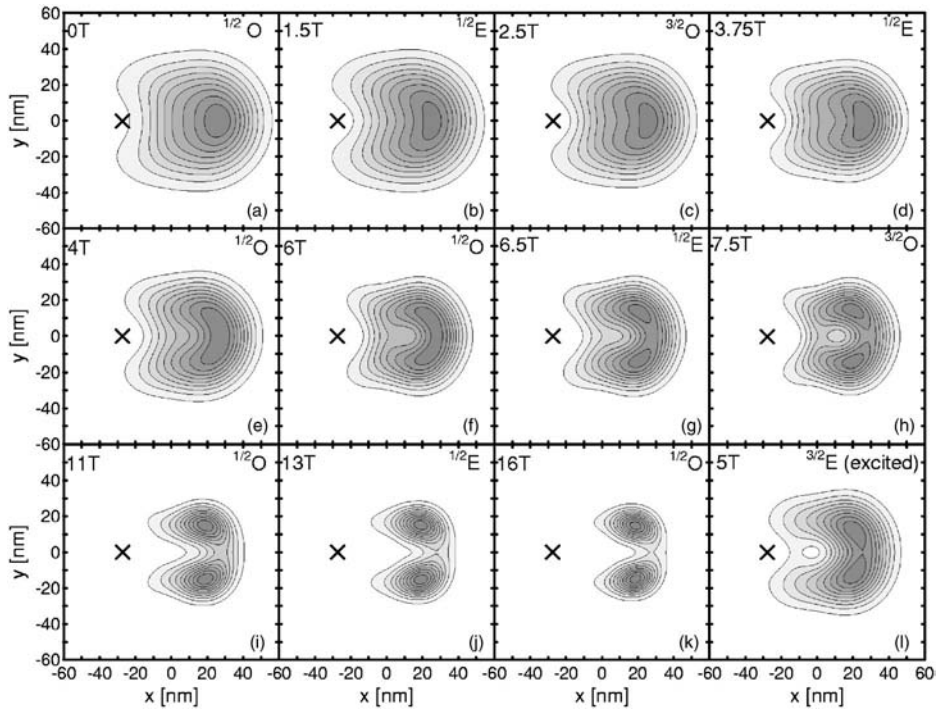

FIG. 5. Pair correlation functions for $d=26.736$ nm and various magnetic fields. One of the electrons is fixed at the position $(-28\ \text{nm}, 0)$ (indicated by the cross). All the plots (a–k) with the exception of the plot (l) for the state $^{3/2}$E at $B=5$ T correspond to the ground state.

the pair correlation plots for the broken-parity states [cf. Figs. 7(g) and 7(h)]. For the electron position fixed in the center of the left dot [see Fig. 7(h)], the two other electrons are more firmly localized in the right dot than in the odd parity state [Fig. 7(f)]. In the broken-parity state, a displacement of the fixed position electron to the position of one of the two charge maxima occupied in the configuration with two electrons in the left dot induces a rotation of the electrons in the right dot [cf. Fig. 7(g)]. Note that due to this rotation the electron charge localized in the lower part of the right dot tunnels through the barrier to the left of the $y=0$ axis. For $d=26.736$ and $B=8.75$ T the tunnel coupling between the dots is still not negligible (see Fig. 2).

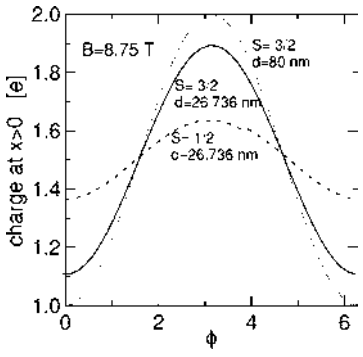

FIG. 6. Charge accumulated in the right quantum dot for the broken-parity Hamiltonian eigenstates as function of the phase of the superposition [Eq. (7)] for $S=1/2$ (dashed line) and $S=3/2$ (solid line) at $d=26.736$ nm and for the spin-polarized state at $d=80$ nm (dotted line).

Let us now look at a spin-polarized broken-parity state for $d=40$ nm and $B=8.4$ T, i.e., in the neighborhood of the border of the phase diagram of Fig. 2, beyond which tunnel coupling is negligible. This specific value of the magnetic field has been chosen because it corresponds to a crossing of spin polarized even and odd energy levels. Although the tunnelling of the electrons from the right to the left dot is not visible in the charge density plot [Fig. 8(a)] the pair correlation plot [Fig. 8(c)] shows that it is not totally absent. Fig. 8(b) shows the lowest triplet state for the reference two-electron calculation with potential (6). The separation of the charges of the two electrons occupying the right quantum dot in the reference calculation is stronger than in the three-electron plot of Fig. 8(a).

Figure 9 shows the results for $d=60$ nm and $B=8.5$ T deep inside the region of vanishing tunnel coupling on the phase diagram presented in Fig. 2. The ellipsoidal deformation of the charge confined in the left dot is visibly smaller than in the preceding plots [see Figs. 7(c) and 8(a)]. The charge density confined in the right quantum dot [Fig. 9(a)] is more similar to the reference two-electron calculations [Fig. 9(b)] than for $d=40$ nm. No tunnel coupling is observed either in the charge density or in the pair correlation plots. After the disappearance of the tunnel effect, the Coulomb coupling of the charge in both dots is still accompanied by quantum interdot correlations in the electron positions [compare Figs. 9(c) and 9(d)].

For $d=80$ nm and $B=8.5$ T, the charge density in the right quantum dot [Fig. 10(a)] becomes identical to the two-electron quantum dot perturbed by an external Coulomb potential [Fig. 10(b)]. The same shape is also reproduced by the pair correlation function for an electron placed in the left dot

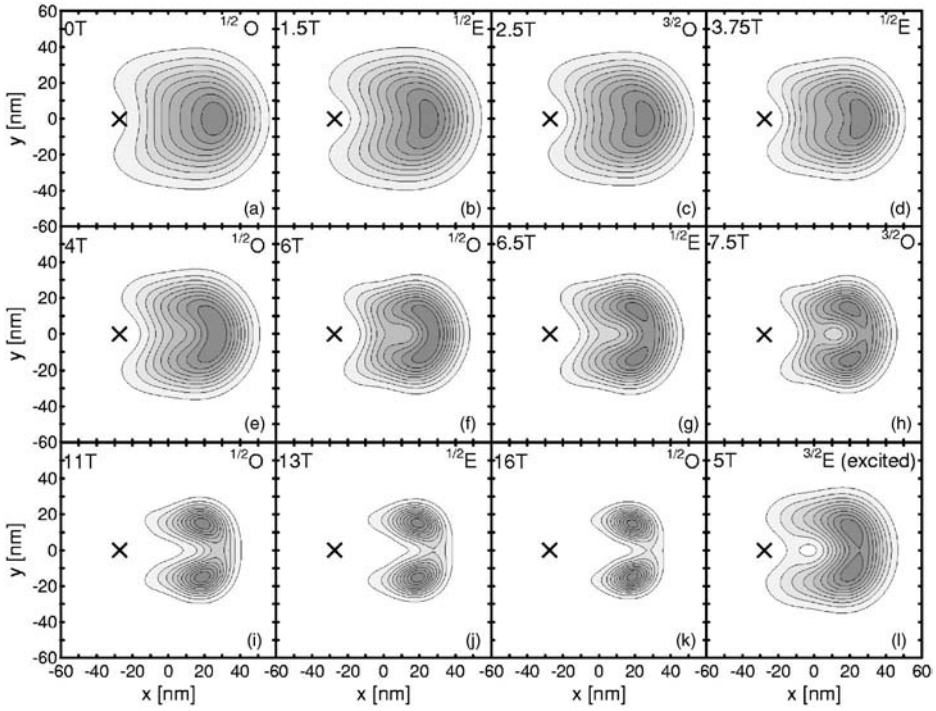

FIG. 5. Pair correlation functions for $d=26.736$ nm and various magnetic fields. One of the electrons is fixed at the position $(-28\ \text{nm}, 0)$ (indicated by the cross). All the plots (a–k) with the exception of the plot (l) for the state $^{3/2}$E at $B=5$ T correspond to the ground state.

the pair correlation plots for the broken-parity states [cf. Figs. 7(g) and 7(h)]. For the electron position fixed in the center of the left dot [see Fig. 7(h)], the two other electrons are more firmly localized in the right dot than in the odd parity state [Fig. 7(f)]. In the broken-parity state, a displacement of the fixed position electron to the position of one of the two charge maxima occupied in the configuration with two electrons in the left dot induces a rotation of the electrons in the right dot [cf. Fig. 7(g)]. Note that due to this rotation the electron charge localized in the lower part of the right dot tunnels through the barrier to the left of the $y=0$ axis. For $d=26.736$ and $B=8.75$ T the tunnel coupling between the dots is still not negligible (see Fig. 2).

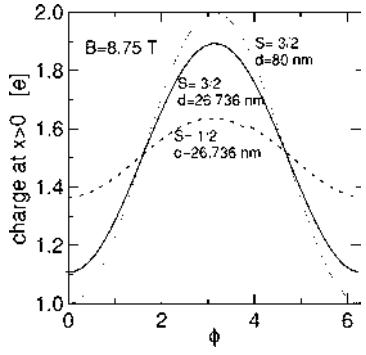

FIG. 6. Charge accumulated in the right quantum dot for the broken-parity Hamiltonian eigenstates as function of the phase of the superposition [Eq. (7)] for $S=1/2$ (dashed line) and $S=3/2$ (solid line) at $d=26.736$ nm and for the spin-polarized state at $d=80$ nm (dotted line).

Let us now look at a spin-polarized broken-parity state for $d=40$ nm and $B=8.4$ T, i.e., in the neighborhood of the border of the phase diagram of Fig. 2, beyond which tunnel coupling is negligible. This specific value of the magnetic field has been chosen because it corresponds to a crossing of spin polarized even and odd energy levels. Although the tunnelling of the electrons from the right to the left dot is not visible in the charge density plot [Fig. 8(a)] the pair correlation plot [Fig. 8(c)] shows that it is not totally absent. Fig. 8(b) shows the lowest triplet state for the reference two-electron calculation with potential (6). The separation of the charges of the two electrons occupying the right quantum dot in the reference calculation is stronger than in the three-electron plot of Fig. 8(a).

Figure 9 shows the results for $d=60$ nm and $B=8.5$ T deep inside the region of vanishing tunnel coupling on the phase diagram presented in Fig. 2. The ellipsoidal deformation of the charge confined in the left dot is visibly smaller than in the preceding plots [see Figs. 7(c) and 8(a)]. The charge density confined in the right quantum dot [Fig. 9(a)] is more similar to the reference two-electron calculations [Fig. 9(b)] than for $d=40$ nm. No tunnel coupling is observed either in the charge density or in the pair correlation plots. After the disappearance of the tunnel effect, the Coulomb coupling of the charge in both dots is still accompanied by quantum interdot correlations in the electron positions [compare Figs. 9(c) and 9(d)].

For $d=80$ nm and $B=8.5$ T, the charge density in the right quantum dot [Fig. 10(a)] becomes identical to the two-electron quantum dot perturbed by an external Coulomb potential [Fig. 10(b)]. The same shape is also reproduced by the pair correlation function for an electron placed in the left dot

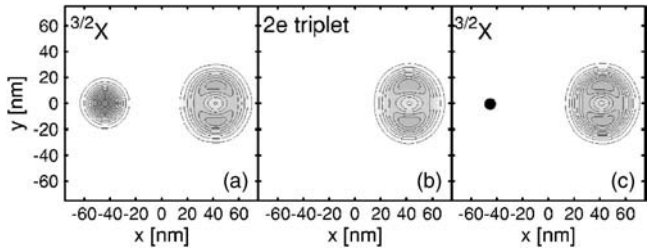

FIG. 10. Charge density (a) and pair correlation functions (c) plots for the spin-polarized broken-parity state for $d=80$ nm at $B=8.5$ T. Charge density of the two-electron spin polarized state in a single dot with a point repulsive center at 80 nm from the center of the dot plotted in (b). In (c) an electron is fixed at (−44, 0 nm)—marked by a dot.

field. The phase diagram for the spatial and spin parities of the ground state as function of the interdot distance and external magnetic field was determined. Near degeneracy of the ground state with respect to parity was used as a criterion for the disappearance of the tunnel coupling between the dots occurring for large interdot distances and/or at high magnetic fields. The three-electron system in laterally coupled dots reproduces the ground-state spin and parity symmetries of circular quantum dots. The exception to this rule is the absence of the spin-polarized even parity ground state which in circular quantum dots has angular momentum $-6\hbar$ and which in laterally coupled dots turns out to be overcorrelated, i.e., correlated more strongly than the ground state. After the disappearance of tunnel coupling the spectrum exhibits spin oscillations that can be described using a model of a two-electron quantum dot perturbed by the Coulomb potential of a spectator electron localized in the other dot. We have shown that interdot electron correlations are present after the extinction of the tunnel coupling. For larger interdot distances quantum interdot correlation disappears although electrostatic interdot coupling is still significant. The effect of the Coulomb interdot coupling for the singly occupied dot is trivial, leading to a shift of the single-electron charge off the dot's center. On the other hand the Coulomb coupling induces pinning of the magnetic-field induced two-electron Wigner molecules, i.e., their extraction from the internal coordinates of the two-electron system to the laboratory frame of reference.

ACKNOWLEDGMENTS

This paper was partly supported by the Flemish Science Foundation (FWO-Vl), the Belgian Science Policy, the University of Antwerpen (VIS and GOA). BS is supported by the EC Marie Curie IEF Project No. MEIF-CT-2004-500157.

[1] B. Partoens and F. M. Peeters, Phys. Rev. Lett. **84**, 4433 (2000).
[2] M. Pi, A. Emperador, M. Barranco, F. Garcias, K. Muraki, S. Tarucha, and D. G. Austing, Phys. Rev. Lett. **87**, 066801 (2001).
[3] D. G. Austing, S. Tarucha, H. Tamura, K. Muraki, F. Ancilotto, M. Barranco, A. Emperador, R. Mayol, and M. Pi, Phys. Rev. B **70**, 045324 (2004).
[4] G. Burkard, G. Seelig, and D. Loss, Phys. Rev. B **62**, 2581 (2000).
[5] S. Bednarek, T. Chwiej, J. Adamowski, and B. Szafran, Phys. Rev. B **67**, 205316 (2003).
[6] D. Bellucci, M. Rontani, F. Troiani, G. Goldoni, and E. Molinari, Phys. Rev. B **69**, 201308(R) (2004).
[7] B. Partoens, A. Matulis, and F. M. Peeters, Phys. Rev. B **59**, 1617 (1999).
[8] J. J. Palacios and P. Hawrylak, Phys. Rev. B **51**, 1769 (1995).
[9] S. C. Benjamin and N. F. Johnson, Phys. Rev. B **51**, 14 733 (1995).
[10] H. Imamura, P. A. Maksym, and H. Aoki, Phys. Rev. B **53**, 12 613 (1996).
[11] M. Rontani, S. Amaha, K. Muraki, F. Manghi, E. Molinari, S. Tarucha, and D. G. Austing, Phys. Rev. B **69**, 085327 (2004).
[12] G. Burkard, D. Loss, and D. P. DiVincenzo, Phys. Rev. B **59**, 2070 (1999).
[13] X. Hu and S. Das Sarma, Phys. Rev. A **61**, 062301 (2000).
[14] A. Harju, S. Siljamäki, and R. M. Nieminen, Phys. Rev. Lett. **88**, 226804 (2002).
[15] M. Marlo, A. Harju, and R. M. Nieminen, Phys. Rev. Lett. **91**, 187401 (2003).
[16] B. Szafran, F. M. Peeters, and S. Bednarek, Phys. Rev. B **70**, 205318 (2004).
[17] C. Yannouleas and U. Landman, Phys. Rev. Lett. **82**, 5325 (1999).
[18] S. Nagaraja, J.-P. Leburton, and R. M. Martin, Phys. Rev. B **60**, 8759 (1999).
[19] R. Ravishankar, P. Matagne, J. P. Leburton, R. M. Martin, and S. Tarucha, Phys. Rev. B **69**, 035326 (2004).
[20] A. Wensauer, O. Steffens, M. Suhrke, and U. Rössler, Phys. Rev. B **62**, 2605 (2000).
[21] J. Kolehmainen, S. M. Reimann, M. Koskinen, and M. Manninen, Eur. Phys. J. B **13**, 731 (2000).
[22] C. Yannouleas and U. Landman, Eur. Phys. J. D **16**, 373 (2001).
[23] F. R. Waugh, M. J. Berry, D. J. Mar, R. M. Westervelt, K. L. Campman, and A. C. Gossard, Phys. Rev. Lett. **75**, 705 (1995).
[24] A. W. Holleitner, C. R. Decker, H. Qin, K. Eberl, and R. H. Blick, Phys. Rev. Lett. **87**, 256802 (2001).
[25] J. M. Elzerman, R. Hanson, J. S. Greidanus, L. H. Willems van Beveren, S. De. Franceschi, L. M. K. Vandersypen, S. Tarucha, and L. P. Kouwenhoven, Phys. Rev. B **67**, 161308(R) (2003).
[26] D. Loss and D. P. DiVincenzo, Phys. Rev. A **57**, 120 (1998).
[27] S. Bednarek, B. Szafran, and J. Adamowski, Phys. Rev. B **65**, 035316 (2001).
[28] S. M. Reimann and M. Manninen, Rev. Mod. Phys. **74**, 1283 (2002).
[29] P. A. Maksym and T. Chakraborty, Phys. Rev. B **45**, R1947 (1992).
[30] P. Hawrylak, and D. Pfannkuche, Phys. Rev. Lett. **70**, 485 (1993).
[31] S. R. Eric Yang, A. H. MacDonald, and M. D. Johnson, Phys. Rev. Lett. **71**, 3194 (1993).

[32] J. J. Palacios, L. Martin-Moreno, G. Chiappe, E. Louis, and C. Tejedor, Phys. Rev. B **50**, R5760 (1994).
[33] M. Eto, Jpn. J. Appl. Phys., Part 1 **36**, 3924 (1997).
[34] P. A. Maksym, Phys. Rev. B **53**, 10 871 (1996).
[35] A. Wójs and P. Hawrylak, Phys. Rev. B **56**, 13 227 (1997).
[36] M. Manninen, S. Viefers, M. Koskinen, and S. M. Reimann, Phys. Rev. B **64**, 245322 (2001).
[37] S. A. Mikhailov and N. A. Savostianova, Phys. Rev. B **66**, 033307 (2002).
[38] M. B. Tavernier, E. Anisimovas, F. M. Peeters, B. Szafran, J. Adamowski, and S. Bednarek, Phys. Rev. B **68**, 205305 (2003).
[39] P. A. Maksym, H. Immamura, G. P. Mallon, and H. Aoki, J. Phys.: Condens. Matter **12**, R299 (2000).
[40] M. Manninen, M. Koskinen, S. M. Reimann, and B. Mottelson, Eur. Phys. J. D **16**, 381 (2001).
[41] B. Szafran, F. M. Peeters, S. Bednarek, and J. Adamowski, Phys. Rev. B **69**, 125344 (2004).
[42] A. Harju, E. Räsanen, H. Saarikoski, M. J. Puska, R. M. Nieminen, and K. Niemelä, Phys. Rev. B **69**, 153101 (2004).
[43] B. Reusch and R. Egger, Europhys. Lett. **64**, 84 (2003).
[44] A. D. Güçlü, J.-S. Wang, and H. Guo, Phys. Rev. B **68**, 035304 (2003).
[45] B. Szafran and F. M. Peeters, Europhys. Lett. **66**, 701 (2004).
[46] C. Yannouleas and U. Landman, Phys. Rev. B **66**, 115315 (2002).
[47] J. Kainz, S. A. Mikhailov, A. Wensauer, and U. Rösser, Phys. Rev. B **65**, 115305 (2002).
[48] B. Szafran, S. Bednarek, J. Adamowski, M. B. Tavernier, E. Anisimovas, and F. M. Peeters, Eur. Phys. J. D **28**, 373 (2004).
[49] C. G. Bao, W. Y. Ruan, and Y. Y. Liu, Phys. Rev. B **53**, 10 820 (1996).
[50] K. Jauregui, W. Häusler, and B. Kramer, Europhys. Lett. **24**, 581 (1993).
[51] W. Häusler and B. Kramer, Phys. Rev. B **47**, 16 353 (1993).
[52] P. S. Drouvelis, P. Schmelcher, and F. K. Diakonos, Phys. Rev. B **69**, 155312 (2004).
[53] M. Wagner, U. Merkt, and A. V. Chaplik, Phys. Rev. B **45**, R1951 (1992).
[54] B. Szafran, F. M. Peeters, S. Bednarek, T. Chwiej, and J. Adamowski, Phys. Rev. B **70**, 035401 (2004).
[55] V. M. Bedanov and F. M. Peeters, Phys. Rev. B **49**, 2667 (1994).